Exotic and excited-state radiative transitions in charmonium from lattice QCD

Jozef J. Dudek,[1,2,*] Robert G. Edwards,[1] and Christopher E. Thomas[1]

[1]*Jefferson Laboratory, 12000 Jefferson Avenue, Newport News, Virginia 23606, USA*

[2]*Department of Physics, Old Dominion University, Norfolk, Virginia 23529, USA*

(Received 20 February 2009; published 15 May 2009)

We compute, for the first time using lattice QCD methods, charmonium radiative transition rates involving states of high spin and exotics. Utilizing a large basis of interpolating fields we are able to project out various excited-state contributions to three-point correlators computed on quenched anisotropic lattices. In the first lattice QCD calculation of the exotic 1^{-+} η_{c1} radiative decay, we find a large partial width $\Gamma(\eta_{c1} \to J/\psi\gamma) \sim 100$ keV. We find clear signals for electric dipole and magnetic quadrupole transition form factors in $\chi_{c2} \to J/\psi\gamma$, calculated for the first time in this framework, and study transitions involving excited ψ and $\chi_{c1,2}$ states. We calculate hindered magnetic dipole transition widths without the sensitivity to assumptions made in model studies and find statistically significant signals, including a nonexotic vector hybrid candidate $Y_{\mathrm{hyb?}} \to \eta_c\gamma$. As well as comparison to experimental data, we discuss in some detail the phenomenology suggested by our results and the extent to which it mirrors that of quark-potential models, and make suggestions for the interpretation of our results involving exotic quantum numbered states.

DOI: 10.1103/PhysRevD.79.094504 PACS numbers: 12.38.Gc, 13.20.Gd, 13.40.Hq, 12.39.Mk

I. INTRODUCTION

The charmonium system is often described as the ''hydrogen atom'' of meson spectroscopy. Being reasonably nonrelativistic, it is explained fairly well by potential models, at least below the open-charm ($D\bar{D}$) threshold. More recently, it has also been studied using effective field theory approaches (such as potential nonrelativistic QCD) and QCD sum rules. Lately there has been a resurgence of interest in the charmonium system, with the *B*-factories, CLEO-c, and BES finding missing states, making more accurate measurements of properties of these states, and discovering a number of new resonances that are not easily explained by the quark model. This has spurred renewed theoretical interest with much speculation as to whether these states are hybrids or multiquark/molecular mesons. To date, there are no charmonium states having manifestly exotic J^{PC}, such as 1^{-+}, 0^{+-}, 2^{+-}, that would directly signal physics not present in potential models.

The states below open-charm ($D\bar{D}$) threshold cannot decay via an Okubo-Zweig-Iizuka allowed strong decay and so have reasonably narrow widths. Their radiative transitions can therefore have significant branching ratios and are experimentally accessible. The transitions from and production of the, as yet unobserved, exotic 1^{-+} are particularly interesting. A lattice calculation of transition form factors of excited charmonia is therefore timely, and this is the first such study. The corresponding excited charmonium spectrum was calculated in lattice QCD in Ref. [1]. Transition form factors of the lightest few charmonia, those ground states accessible with interpolating fields $\bar{\psi}\Gamma\psi$, were calculated in Ref. [2]. This work brought to the attention of CLEO-c experimentalists the discrepancy between the lattice calculated value of $\Gamma(J/\psi \to \eta_c\gamma)$ (and indeed the values predicted in most model calculations) and the single experimental measurement of this from Crystal Ball [3]. In a tour-de-force analysis [4], a much more reliable value was extracted from CLEO-c data that is in much better agreement with theoretical estimates.

The calculation we will present is performed in the quenched approximation, neglecting altogether the effect of light-quark degrees of freedom. As such, it is rather directly related to the simplest quark-potential models in which charm quarks move in a static potential of assumed gluonic origin. Attempts have been made to add in the effects of light-quark loops to these models [5–7], in some cases finding that these effects can be large [8]. We will address this possibility in light of our results.

A strong motivation for developing the lattice QCD techniques required to extract excited- and exotic-state radiative transition matrix elements is the versatility of the method. We can use these methods, tested here in charmonium, at any computationally feasible quark mass. In particular, this opens up the possibility of computing, in a framework close to QCD, the meson photocouplings that appear in the meson photo-production process to be utilized in the JLab 12 GeV GlueX experiment [9]. In this paper we will also compare results with the flux-tube model of gluonic excitations, which to date is the only theoretical guide to the size of the hybrid couplings and hence production rates [10,11].

The paper is structured as follows: We begin in Sec. II with a description of the technology used to construct three-point correlators and to project onto the contribution due to various excited states. In Sec. III we present our results for the transition form factors between various

*dudek@jlab.org

meson states. A discussion of the phenomenology of these results, in terms of experiment and models, follows in Sec. IV before we conclude in Sec. V. Two appendixes which consider some technical details complete the manuscript.

II. TECHNOLOGY

In this paper we will explore radiative transitions with charm-mass quarks using the quenched anisotropic lattices and clover fermion action described in [1]. Radiative transition matrix elements follow from vector current three-point functions, whose construction using sequential-source technology is described in [2]. As in [2], only connected diagrams are considered, with the assumption that disconnected diagrams are negligible in comparison. The new item of technology in this study is the use of a large basis of meson interpolating fields as explored in two-point functions in [1] with further interpretation in [12].

The operators utilized are lattice-discretized versions of the gauge-invariant fermion bilinears,

$$\bar{\psi}(x)\Gamma\overleftrightarrow{D}_i\overleftrightarrow{D}_j\ldots\psi(x),$$

where $\overleftrightarrow{D} = \overleftarrow{D} - \overrightarrow{D}$ is the gauge-covariant derivative operator. In order to improve the overlap onto lower-lying mesons, the quark fields may also be smeared over space as $e^{(1/4)\sigma^2 D_i D_i}\psi(x)$. Linear combinations of these basic operators have been constructed which transform irreducibly under the lattice cubic symmetry and which have rather simple interpretations in the limit of zero lattice spacing; for details see [1,12]. The operator set is large enough to have a considerable redundancy within a given quantum number sector, which can be utilized to extract excited states.

A. "Ideal" operators and eigenvector projection

In [1] the spectrum of charmonium was extracted by solution of the generalized eigenvalue problem[1]

$$C_{ij}(t)v_j^{\mathfrak{n}} = \lambda_{\mathfrak{n}}(t)C_{ij}(t_0)v_j^{\mathfrak{n}}, \qquad \lambda_{\mathfrak{n}}(t) \underset{(t\gg t_0)}{\longrightarrow} e^{-E_{\mathfrak{n}}(t-t_0)},$$
$$v_i^{\mathfrak{n}*}C_{ij}(t_0)v_j^{\mathfrak{m}} = \delta_{\mathfrak{n}\mathfrak{m}}, \tag{1}$$

which constitutes the best solution for the spectrum in the variational sense. The matrix of two-point correlators is constructed as $C_{ij}(t) = \langle 0|\sum_{\vec{x}}\mathcal{O}_i(\vec{x},t)\mathcal{O}_j(\vec{0},0)|0\rangle$, where the sum over lattice sites forces the three-momentum of single particle states to be zero.[2] This method relies upon a redundancy of operators $\mathcal{O}_i$ in any given quantum number sector.

Fitting the time dependence of principal correlators, $\lambda_{\mathfrak{n}}(t)$, gives us the masses (or energies at finite three-momentum) of the states with the quantum numbers of the Hermitian operators $\mathcal{O}_{i,j}$. Details of the two-point analysis, including the importance of the choice of time slice t_0, are given in [1]. The interpretation of the eigenvector $v^{\mathfrak{n}}$ in the solution of Eq. (1) can be expressed as follows: weighting the operators by this vector gives the optimal operator, within the limited operator space, for the state labeled by $\mathfrak{n}$. It is convenient to normalize these ideal operators in a manner which accounts for the value of t_0: $\Omega^{\mathfrak{n}} = \sqrt{2E_{\mathfrak{n}}}e^{-E_{\mathfrak{n}}t_0/2}v_i^{\mathfrak{n}}\mathcal{O}_i$.

Note that these eigenvectors are trivially related to the vacuum-operator-state matrix elements or "overlaps," $Z_i^{\mathfrak{n}} = \langle\mathfrak{n}|\mathcal{O}_i|0\rangle$, that appear in a bound-state spectral decomposition,

$$C_{ij}(t) = \sum_{\mathfrak{n}}\frac{Z_i^{\mathfrak{n}*}Z_j^{\mathfrak{n}}}{2E_{\mathfrak{n}}}e^{-E_{\mathfrak{n}}t},$$

by $Z_j^{\mathfrak{n}}v_j^{\mathfrak{m}} = \sqrt{2E_{\mathfrak{n}}}e^{E_{\mathfrak{n}}t_0/2}\delta_{\mathfrak{n},\mathfrak{m}}$ or

$$Z_j^{\mathfrak{n}} = \sqrt{2E_{\mathfrak{n}}}e^{E_{\mathfrak{n}}t_0/2}v_i^{\mathfrak{n}*}C_{ij}(t_0). \tag{2}$$

The procedure we shall follow in this paper is to compute three-point correlators having at the source (located on a fixed time slice, t_i) a (smeared) local operator of the form $\bar{\psi}(\vec{0},t_i)\Gamma\psi(\vec{0},t_i)$—all possible gamma matrices can be considered for the computing cost of a single "forward" propagator. In this work we consider $\Gamma = \gamma_5, \gamma_i, 1$, giving access to pseudoscalar, vector, and scalar states at the source.

At the sink (located on a fixed time slice, t_f) we use sequential-source technology using a broad selection of local and derivative-based operators as described in [1]—for each operator at a given momentum (usually $\vec{p}_f = 000$) we have the computing cost of a single "backward" propagator. At the vector current insertion (inserted on all time slices $t_i < t < t_f$) we insert the local vector current with all possible lattice three-momenta $\vec{q}$ up to $|\vec{q}|^2 = 4$. Translational invariance ensures momentum conservation, selecting the correct value of $\vec{p}_i$ out of the sum over all momenta produced by a local operator.

$$C_{\Gamma\mu j}(\vec{p}_i,\vec{p}_f;t_i,t,t_f) = \left\langle 0\left|\sum_{\vec{z}}e^{-i\vec{p}_f\cdot\vec{z}}\mathcal{O}_j(\vec{z},t_f)\cdot\sum_{\vec{y}}e^{i\vec{q}\cdot\vec{y}}j_\mu(\vec{y},t)\right.\right.$$
$$\left.\left.\cdot\,\bar{\psi}(\vec{0},t_i)\Gamma\psi(\vec{0},t_i)\right|0\right\rangle. \tag{3}$$

Three-point correlators for ideal operators are constructed from the "raw" correlators, Eq. (3), by projecting with the appropriate eigenvector,[3]

[1] Repeated indices are summed.

[2] In some cases we also considered nonzero three-momentum correlators—this will be discussed later.

[3] A somewhat different application of the same basic idea has recently been presented in [13].

$$C_{\Gamma\mu\mathfrak{n}}(\vec{p}_i, \vec{p}_f; t_i, t, t_f) = \left\langle 0 \left| \sum_{\vec{z}} e^{-i\vec{p}_f\cdot\vec{z}} \Omega^{\mathfrak{n}}(\vec{z}, t_f) \cdot \sum_{\vec{y}} e^{i\vec{q}\cdot\vec{y}} j_\mu(\vec{y}, t) \cdot \bar{\psi}(\vec{0}, t_i)\Gamma\psi(\vec{0}, t_i) \right| 0 \right\rangle = \sqrt{2E_{\mathfrak{n}}} e^{-E_{\mathfrak{n}} t_0/2} v_j^{\mathfrak{n}*} C_{\Gamma\mu j}(\vec{p}_i, \vec{p}_f; t_i, t, t_f).$$

The net effect is to provide us with a three-point correlator that, while it has multiple states contributing through the local source operator $\bar{\psi}(\vec{0}, t_i)\Gamma\psi(\vec{0}, t_i)$, should have only a single state, $\mathfrak{n}$, contributing from the sink operator $\Omega^{\mathfrak{n}}$. In principle, we could improve this further by using the full basis of operators at the source as well as the sink, but using sequential-source technology this quickly becomes rather expensive.[4]

In fact, we can be a little more precise about the statement that only a single state contributes at the sink—in considering the analysis of the two-point correlators, we determined that t_0 can be considered to be the time slice on which the correlator matrix (of dimension N) is saturated by N states; closer to the operator we require more states to describe the correlator matrix [1,14]. It follows that if we are t_0 time slices away from the sink operator position t_f, we can be quite confident that we have contribution only from the single state labeled by $\mathfrak{n}$. When we go to fit the time dependence of the three-point correlator, we will not use time slices any closer to the sink than $t = t_f - t_0$.

In Fig. 1 we show the effect of the eigenvector projection onto ideal states in the case of a pseudoscalar source operator $\bar{\psi}\gamma^5\psi$ and a selection of pseudoscalar sink operators. We clearly see that the projection onto the ground-state ideal operator produces a considerable "flattening" of the correlator moving toward the sink. We do see some curvature beginning within $t_0 = 8$ time slices away from the sink, as expected.[5] More importantly, for this study we see that projection onto the ideal operator for the *first excited state* yields a clear nonzero signal from which one can extract a transition matrix element.

There is a slight technical subtlety to be dealt with in the eigenvector projection onto ideal operators that arises from the method of solution of the two-point problem. Solving the eigenvalue problem gives eigenvectors on each time slice, $v_j^{\mathfrak{n}}(t_{2\mathrm{pt}})$—if the solution is to be a true spectral representation, there should be no time dependence in the eigenvectors, at least for $t_{2\mathrm{pt}} > t_0$ where the correlator

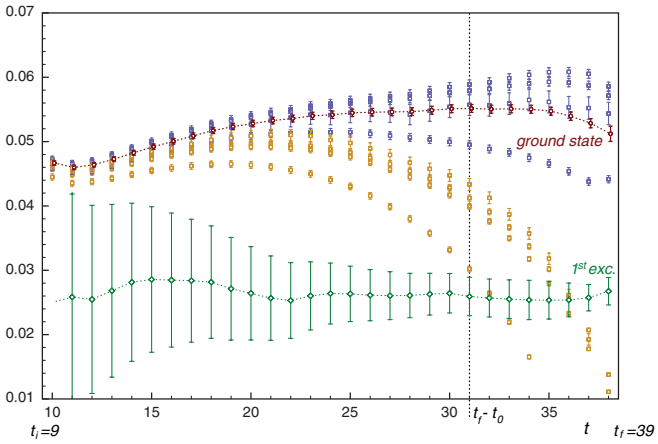

FIG. 1 (color online). Blue and yellow data—suitably normalized pseudoscalar-vector current-pseudoscalar correlators for a set of different sink operators. Red data—formed by projection with the ground-state eigenvector $v_i^{(0)}$. Green data—formed by projection with the first excited-state eigenvector $v_i^{(1)}$.

matrix is supposed to be saturated. In [1] we saw that over a considerable range of $t_{2\mathrm{pt}}$, the Z values [obtained trivially from the v; see Eq. (2)] were flat. We explore the effect of any such possible time dependence on the three-point functions by performing the projection for eigenvectors belonging to a range of time slices, $v_j^{\mathfrak{n}}(t_{2\mathrm{pt}})$. In Fig. 2 we show for a ground-state and first excited-state projection the $t_{2\mathrm{pt}}$ dependence on the projected correlator. It is clear that there is no strong dependence on $t_{2\mathrm{pt}}$, and we choose to average over the projections for various $t_{2\mathrm{pt}}$ to reduce configuration-by-configuration fluctuations that may be caused by the generalized eigensystem solver.

B. Transition form factors

The ideal operator-projected three-point functions are related to the transition matrix elements between states as

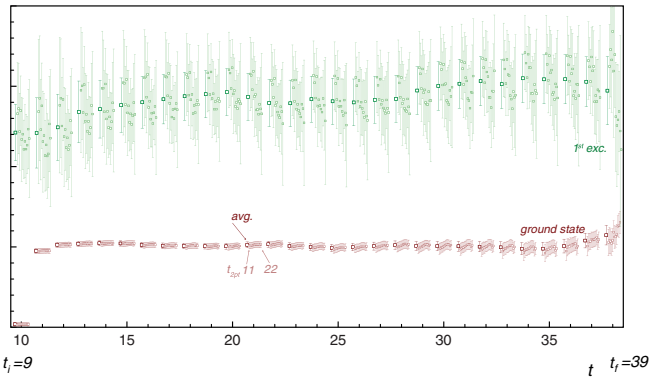

FIG. 2 (color online). Eigenvector projected correlators as a function of current insertion time t. For each t value we show the result of projecting with each of $v_i^{\mathfrak{n}=0,1}(t_{2\mathrm{pt}})$ for $11 \leq t_{2\mathrm{pt}} \leq 22$. Also shown is the average over the various $t_{2\mathrm{pt}}$ values.

[4]In addition, analysis of these correlators would require detailed knowledge of the finite-momentum behavior of the derivative-based operators—we will consider this in Appendix A and find that it is not entirely trivial.

[5]Indeed, if we fit the time dependence of the curvature at the sink with a single exponential, we find that it corresponds to a mass heavier than the heaviest state extracted from the eight-operator two-point correlation matrix.

follows:

$$C_{\Gamma\mu\mathfrak{n}}(\vec{p}_i,\vec{p}_f;t_i,t,t_f)=\langle 0|\Omega^{\mathfrak{n}}(\vec{0},0)|f_{\mathfrak{n}}(\vec{p}_f)\rangle\frac{e^{-E_{\mathfrak{n}}(t_f-t)}}{2E_{\mathfrak{n}}}\times\sum_{\mathfrak{m}}\langle f_{\mathfrak{n}}(\vec{p}_f)|j^{\mu}(\vec{0},0)|i_{\mathfrak{m}}(\vec{p}_i)\rangle\times\frac{e^{-E_{\mathfrak{m}}(t-t_i)}}{2E_{\mathfrak{m}}}\langle i_{\mathfrak{m}}(\vec{p}_i)|\mathcal{O}_i(\vec{0},0)|0\rangle. \quad (4)$$

While all possible eigenstates with the quantum numbers of $\mathcal{O}_i$ will contribute at the source (the sum over $\mathfrak{m}$), the eigenvector projection ensures that we need only consider the single state $\mathfrak{n}$ at the sink. Our normalization of $\Omega_{\mathfrak{n}}$ ensures that if f is spin zero, $\langle 0|\Omega^{\mathfrak{n}}(\vec{0},0)|f_{\mathfrak{n}}(\vec{p}_f)\rangle = 2E_{\mathfrak{n}}$.

The Minkowski-space transition matrix element $\langle f_{\mathfrak{n}}(\vec{p}_f)|j^{\mu}(\vec{0},0)|i_{\mathfrak{m}}(\vec{p}_i)\rangle$ can be decomposed in terms of multipole form factors multiplied by Lorentz covariant combinations of the momenta and (if appropriate) polarization tensors of the particles labeled by i, f: $\sum_k F_k(Q^2)\kappa_k^{\mu}(p_i,p_f,\epsilon_i,\epsilon_f^*)$. The general technique for obtaining these covariant multipole decompositions is given in the Appendix of [2]. Inserting this decomposition into Eq. (4), and performing the implicit sums over helicity (in the case of spin ≥ 1), the three-point correlator on each time slice t can be expressed as a linear sum of known "kinematic" and "propagation" factors times the unknown multipole form factors,[6]

$$C_{\Gamma\mu\mathfrak{n}}(\vec{p}_i,\vec{p}_f;t_i,t,t_f)=\sum_{\mathfrak{m}}P_{\mathfrak{m},\mathfrak{n}}(\vec{p}_i,\vec{p}_f,t_i,t,t_f)\times\sum_k K^{\mu}_{k,\mathfrak{m},\mathfrak{n}}(\vec{p}_i,\vec{p}_f)F_{k,\mathfrak{m},\mathfrak{n}}(Q^2).$$

In practice, we opt to solve this linear system[7] on each time slice t for a set of "effective," t-dependent form factors, $\tilde{F}_{k\mathfrak{n}}(Q^2,t)$, using the propagation and kinematic factors for the ground state at the source ($\mathfrak{m}=0$):

$$C_{\Gamma\mu\mathfrak{n}}(\vec{p}_i,\vec{p}_f;t_i,t,t_f)=P_{0,\mathfrak{n}}(\vec{p}_i,\vec{p}_f,t_i,t,t_f)\times\sum_k K^{\mu}_{k,0,\mathfrak{n}}(\vec{p}_i,\vec{p}_f)\tilde{F}_{k,\mathfrak{n}}(Q^2,t).$$

The propagation factor $P_{0,\mathfrak{n}}(\vec{p}_i,\vec{p}_f,t_i,t,t_f)$ contains the overlap $Z^0_{\Gamma}(\vec{p}_i)$ and the energy $E_0(\vec{p}_i)$. These are determined in the analysis of a two-point function at finite momentum. Since the state masses at zero momentum are rather precisely determined by the variational solution, we use the continuum dispersion relation to obtain $E(\vec{p}) = \sqrt{m^2+|\vec{p}|^2}$. Z values then follow from a linear fit to the finite-momentum two-point correlators, supplying the known $\exp(-E_{\mathfrak{n}}(\vec{p})t)$ factors.

The extracted effective form factors have the property that $\tilde{F}_{k,\mathfrak{n}}(Q^2,t)\approx F_{k,\mathfrak{n}}(Q^2)+\mathcal{O}(e^{-(E_{\mathfrak{m}=1}-E_{\mathfrak{m}=0})(t-t_i)})$ so that away from the source the excited-state contributions die off and the form factor plateaus to the $i_{\mathfrak{m}=0}\rightarrow f_{\mathfrak{n}}$ value. We fit the time dependence of these extracted effective form factors to a sum of exponentials, where the energy dependence is that extracted from spectrum studies.[8] A typical example is shown in Fig. 3. We retain only the plateau value, discarding the excited-state information at the source.[9]

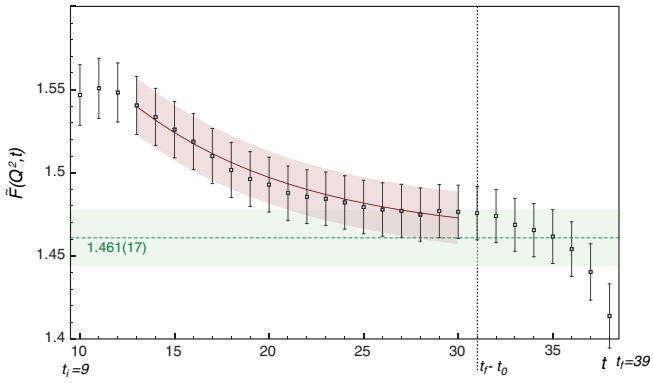

FIG. 3 (color online). Effective time-dependent form factor. The fit with a constant plus a single exponential is shown in red, with the constant fit value shown in green. The fit is linear for the coefficients since the excited-state energies appearing in the exponent are determined from the solution of the two-point function problem.

The expansion of transition matrix elements as performed above relies upon the continuum Lorentz symmetry, which is broken on our cubic lattice. A more rigorous study would consider the expansion in terms of irreducible representations of the cubic group at finite momentum and would typically involve a larger number of form factors, some of which would tend to the multipole form factors as the lattice spacing $a\rightarrow 0$ and some of which would have to vanish. We have not performed such a decomposition but suspect that it is not important at this lattice spacing since, when we solve the correlator-form-factor linear system assuming continuumlike decompositions, we typically obtain χ^2 per d.o.f. very close to 1, suggesting that there is little need to enlarge the basis space.

[6]This is essentially the same decomposition presented in [2].

[7]By jackknifed singular value decomposition as described in [2].

[8]With the exponential dependence supplied, this is a linear fit for the coefficients.

[9]Strictly speaking, the kinematic factors for excited $\mathfrak{m}$ states need not be proportional to the ground-state values, such that excited-state multipoles may "leak" into the wrong ground-state multipole—clearly this effect will fall off for $t\gg t_i$. An alternative approach is to include the excited-state terms directly into the decomposition fit, expanding the space to also be over time slices, the time dependence being the discriminator for the various states contributing at the source—this guarantees the right kinematic factors for excited states. In all cases to be presented, the analysis was cross-checked using this fitting method (the excited-state energies obtained from applying the dispersion relation to the excited-state masses reliably extracted using the variational method) and agreement within statistical fluctuations was found.

The fact that charmonium states are eigenstates of charge conjugation (C), coupled with the photon having $C = -1$, means that all charmonium radiative transitions are between states of opposite C. The origin of this is that the photon couples equally to the charm quark and the charm antiquark. In our lattice calculation we need not impose this symmetry; by coupling only to the quark we can obtain transitions between states of equal C. One way of viewing this is that it is like having a u, d pair but as heavy as the charm quark—this can be useful for comparison with models, and we will show results for a number of C violating transitions.

III. RESULTS

A. Vector current renormalization

Since we use the local vector current in the construction of our three-point functions, we need to determine the renormalization constant Z_V to relate the extracted matrix elements to physical matrix elements. We do this by insisting that the pseudoscalar form factor at zero Q^2 takes the value 1. On an anisotropic lattice we should allow there to be different renormalization constants for temporally and spatially directed currents; indeed, we find $Z_{V(s)} = 1.23(2)$ and $Z_{V(t)} = 1.118(6)$. In all results presented below, only the spatially directed current is used. See Appendix B for a discussion of the effect of improvement of the vector current.

B. Scalar-vector transitions

The first results we will present concern transitions between scalar (0^{++}) and vector (1^{--}) states of charmonium. Using a quark-smeared operator $\bar{\psi}\psi$ at the source and 13 vector operators[10] at the sink, we extracted transitions between the ground-state scalar χ_{c0} and the lowest six vector states. In Table I we show the spectrum reported in [12], possible comparable experimental states, and a model-dependent state assignment.

This transition is characterized by two multipole amplitudes, a transverse electric dipole $E_1(Q^2)$ and a longitudinal $C_1(Q^2)$, the matrix element decomposition being

$$\begin{aligned}\langle S(\vec{p}_S)|j^\mu(0)|V(\vec{p}_V,\lambda)\rangle &= \Omega^{-1}(Q^2)\Big(E_1(Q^2)[\Omega(Q^2)\epsilon^\mu(\vec{p}_V,\lambda) - \epsilon(\vec{p}_V,\lambda)\cdot p_S \\ &\times (p_V^\mu p_V\cdot p_S - m_V^2 p_S^\mu)] + \frac{C_1(Q^2)}{\sqrt{q^2}} m_V \epsilon(\vec{p}_V,\lambda)\cdot p_S \\ &\times [p_V\cdot p_S(p_V+p_S)^\mu - m_S^2 p_V^\mu - m_V^2 p_S^\mu]\Big), \end{aligned} \quad (5)$$

where $\Omega(Q^2) = (p_V\cdot p_S)^2 - m_S^2 m_V^2$.

[10] In the notation of [1] they are the quark-smeared versions of γ_i, $\gamma_i\gamma_0$, $a_0\times\nabla_{T1}$, $a_1\times\nabla_{T1}$, $\rho\times\mathbb{D}_{T1}$, $\rho_{(2)}\times\mathbb{D}_{T1}$, $\pi\times\mathbb{B}_{T1}$, $\pi_{(2)}\times\mathbb{B}_{T1}$ and the unsmeared versions of γ_i, $\gamma_i\gamma_0$, $a_1\times\nabla_{T1}$, $\pi\times\mathbb{B}_{T1}$, $\pi_{(2)}\times\mathbb{B}_{T1}$. In the $\vec{p}_f = (100)$ case the $\rho_{(2)}\times\mathbb{D}$ and $\pi_{(2)}\times\mathbb{B}$ operators were not included.

TABLE I. T_1^{--} spectrum extracted from two-point functions, suggested experimental state analogues, and quark-model bound-state assignments made in [12].

Level	Mass/MeV	Suggested state	Model assignment
0	3106(2)	J/ψ	1^3S_1
1	3746(18)	$\psi'(3686)$	2^3S_1
2	3846(12)	$\psi_3(3^{--})$	Lattice artifact
3	3864(19)	$\psi''(3770)$	1^3D_1
4	4283(77)	ψ("4040")	3^3S_1
5	4400(60)	Y?	Hybrid

The "vector" operators used are, in fact, all in a particular irreducible representation of the cubic group at rest, namely T_1, which in the continuum limit contains spins 1, 3, 4 …. By considering the degeneracy pattern and the values of the overlaps $Z_j^{(n)}$, the two-point function analysis strongly suggests that the second excited state in the T_1^{--} sector is actually a spin-3 state and as such we do not present results involving this state here [1,12]. Additionally, we do not show the amplitudes for the fourth excited state as the signals are statistically consistent with zero for all Q^2. Shown in Fig. 4 are the electric dipole transition form factors for the four relevant states. See Appendix A for a discussion of the inclusion of $\vec{p}_f = (100)$ correlators in this analysis.

In each case the Q^2 dependence of the lattice data has been fitted with the form

$$E_1(Q^2) = E_1(0)(1+\lambda Q^2)e^{-(Q^2/16\beta^2)}, \quad (6)$$

whose motivation is described in [2]. The results of the fits are given in Table II. One point to make here is that, in our lattice calculations, the photon only couples to the quark and not the antiquark, and we do not explicitly include the electric charge of the quark. Therefore, we actually compute and present $\hat{F}_k(Q^2)$ which are related to the physical multipole amplitudes by $F_k(Q^2) = 2\times\frac{2}{3}e\times\hat{F}_k(Q^2)$. Note also that the multipole amplitudes have mass dimension 1 and hence we plot them in temporal lattice units, where $a_t^{-1} = 6.05$ GeV is determined from the static potential. Partial decay widths follow by averaging over initial helicities and summing over final helicities which gives, for a general $A\to B\gamma$ decay,

$$\Gamma(A\to B\gamma) = \frac{1}{2J_A+1}\alpha\frac{16}{9}\frac{|\vec{q}|}{m_A^2}\sum_k|\hat{F}_k(0)|^2.$$

Where we have experimental masses for states, we use these to compute the phase space; otherwise we use the value extracted from the lattice calculation [1,12].

The ground-state transition $\chi_{c0}\to J/\psi\gamma$ form factor shows behavior rather similar to that found in [2], which used the same lattices but domain wall fermions rather than clover and which did not make use of multiple sink operators and operator projection. We will return to this in a little

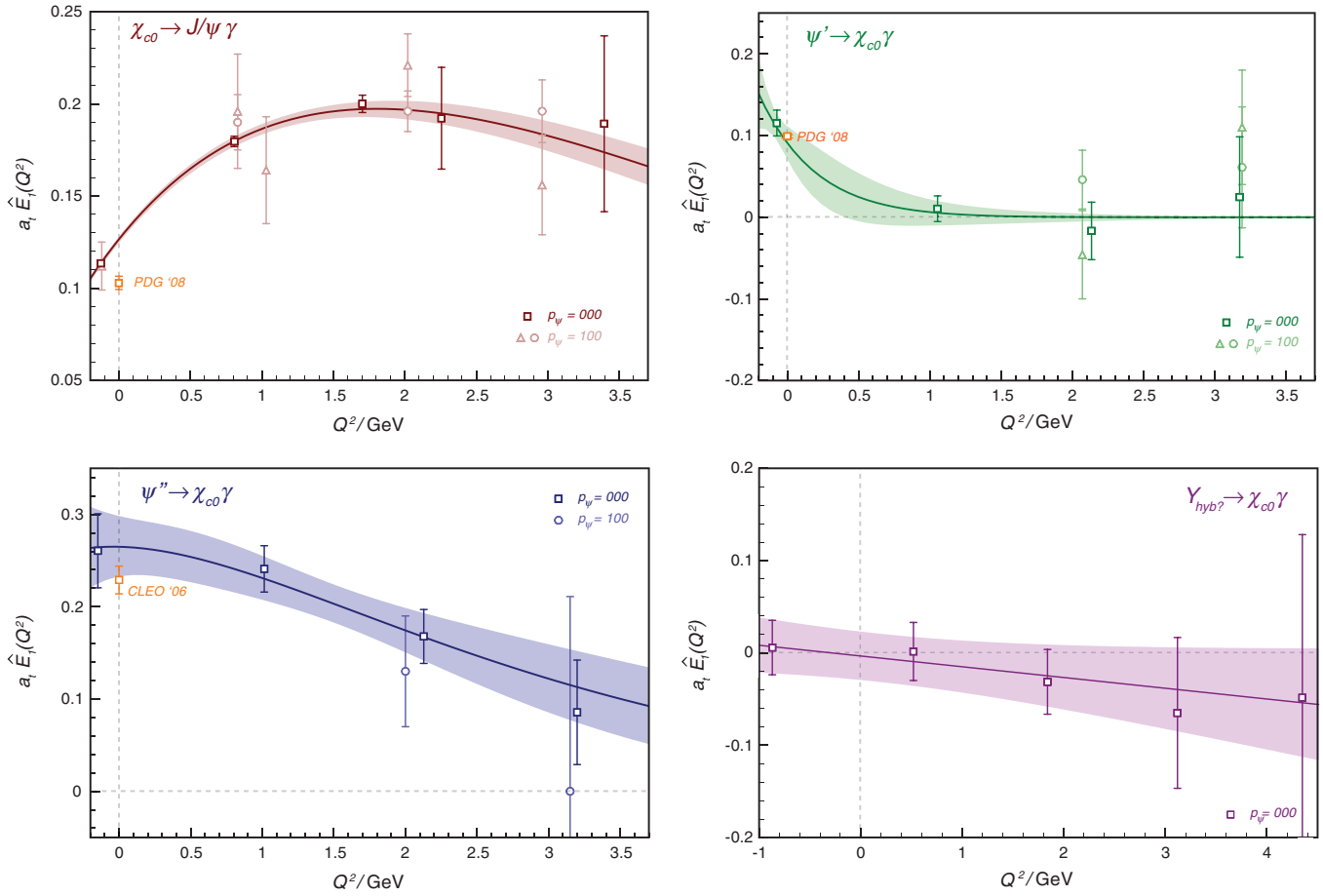

FIG. 4 (color online). Electric dipole transition form factors $\chi_{c0} \leftrightarrow \psi$. Plotted is the form factor in temporal lattice units against the photon virtuality in GeV^2. The fits are to the lattice Q^2 dependence as described in the text. Experimental points at $Q^2 = 0$ are extracted from experimental decay widths taken from [15,16].

more detail in Appendix B, where we will consider the effect of $\mathcal{O}(ma)$ improvement of the local vector current. We will discuss the results in comparison with experiment and with quark-potential models in Sec. IV B.

C. Vector-pseudoscalar transitions

Using the same T_1^{--} operator set at the sink and the quark-smeared $\bar{\psi}\gamma^5\psi$ operator at the source, we obtained results for the single magnetic dipole form factor in the vector-pseudoscalar transition. The decomposition used[11] is

$$\langle P(\vec{p}_P)|j^\mu(0)|V(\vec{p}_V,\lambda)\rangle = \frac{2V(Q^2)}{m_P + m_V}\epsilon^{\mu\alpha\beta\gamma}p_{P\alpha}p_{V\beta}\epsilon_\gamma(\vec{p}_V,\lambda).$$

Figure 5 shows the form factors for the transition between the lightest four vector states [ignoring the suspected 3^{--} intruder and the noisy ψ ("4040") state] and the η_c. The fit form in Eq. (5) was again used, with the fit results presented in Table III. We refer the reader to the paper [2] for a discussion of the systematic error introduced into the phase

TABLE II. Results of the fit to lattice data using Eq. (6). We give the partial decay width computed using the fitted value of $E_1(0)$ and physical phase space (where known). All errors are just lattice statistical. Experimental partial decay widths are from [15,16].

Sink level	Suggested transition	$a_t\hat{E}_1(0)$	β/MeV	λ/GeV^{-2}	$\Gamma_{\rm lat}$/keV	$\Gamma_{\rm expt}$/keV
0	$\chi_{c0} \to J/\psi\,\gamma$	0.127(2)	409(12)	1.14(5)	199(6)	131(14)
1	$\psi' \to \chi_{c0}\gamma$	0.092(19)	164(55)	0 (fixed)	26(11)	30(2)
3	$\psi'' \to \chi_{c0}\gamma$	0.265(33)	324(77)	0.58(56)	265(66)	199(26)
5	$Y_{\rm hyb} \to \chi_{c0}\gamma$	0.00(3)	Linear	Fit	$\lesssim 20$	$\cdots$

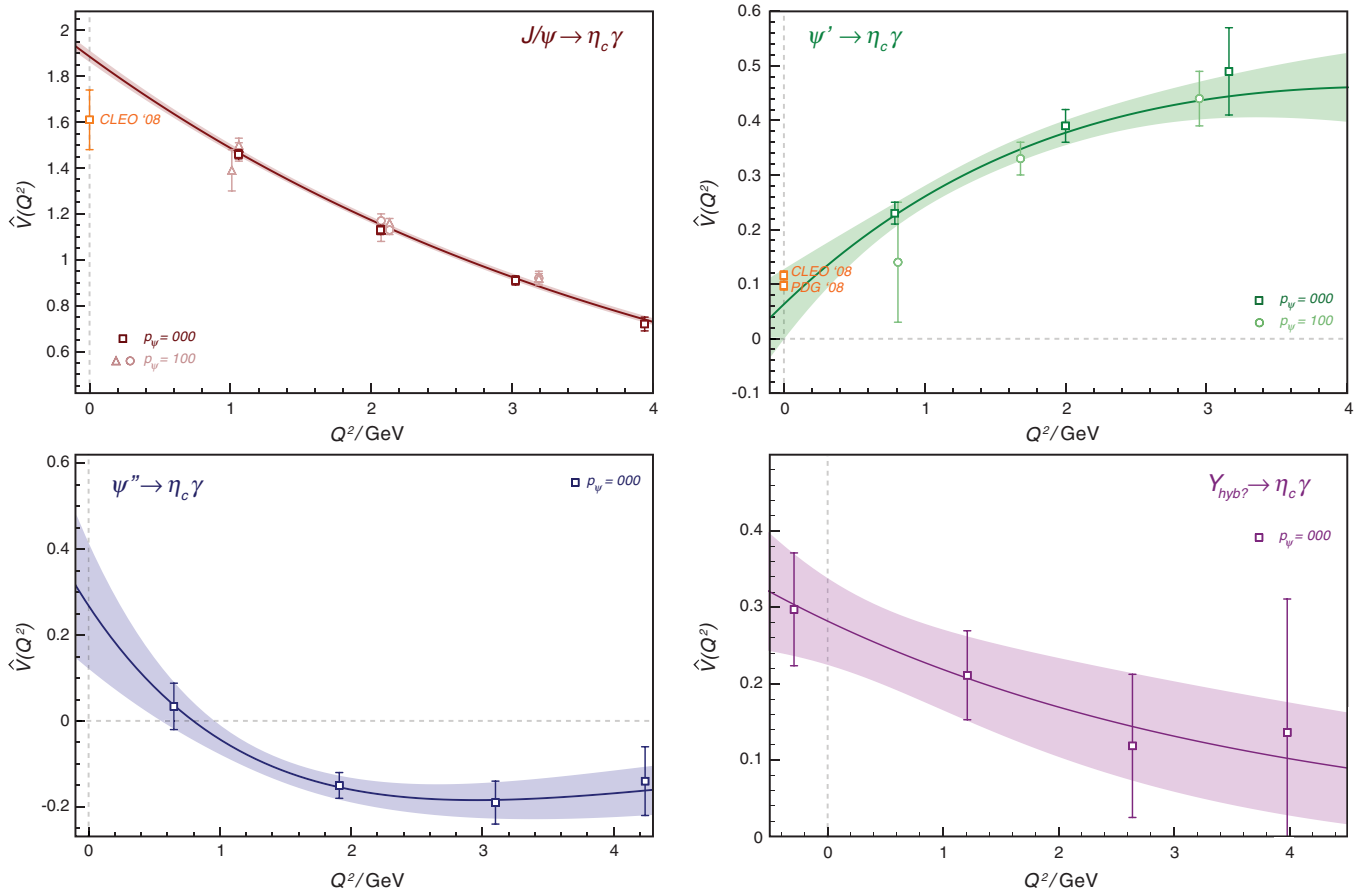

FIG. 5 (color online). Magnetic dipole transition form factors $\psi \rightarrow \eta_c$. Plotted is the dimensionless form factor against the photon virtuality in GeV^2. Fits to the lattice Q^2 dependence are as described in the text. Experimental points at $Q^2 = 0$ are extracted from experimental decay widths taken from [4,15].

space by an inaccurate lattice estimate of the hyperfine splitting.

D. Axial-vector transitions

In transitions between axial (1^{++}) and vector (1^{--}) states there are two transverse form factors, the electric dipole (E_1) and magnetic quadrupole (M_2), and one longitudinal form factor (C_1). The matrix element decomposition takes the form

$$\begin{aligned}\langle A(\vec{p}_A,\lambda_A)|j^\mu(0)|V(\vec{p}_V,\lambda_V)\rangle = \frac{i}{4\sqrt{2}\Omega(Q^2)}\epsilon^{\mu\nu\rho\sigma}(p_A-p_V)_\sigma\Big[E_1(Q^2)(p_A+p_V)_\rho(2m_A[\epsilon^*(\vec{p}_A,\lambda_A)\cdot p_V]\epsilon_\nu(\vec{p}_V,\lambda_V)\\ + 2m_V[\epsilon(\vec{p}_V,\lambda_V)\cdot p_A]\epsilon^*_\nu(\vec{p}_A,\lambda_A)) + M_2(Q^2)(p_A+p_V)_\rho(2m_A[\epsilon^*(\vec{p}_A,\lambda_A)\cdot p_V]\epsilon_\nu(\vec{p}_V,\lambda_V)\\ - 2m_V[\epsilon(\vec{p}_V,\lambda_V)\cdot p_A]\epsilon^*_\nu(\vec{p}_A,\lambda_A)) + \frac{C_1(Q^2)}{\sqrt{q^2}}(-4\Omega(Q^2)\epsilon^*_\nu(\vec{p}_A,\lambda_A)\epsilon_\rho(\vec{p}_V,\lambda_V)\\ + (p_A+p_V)_\rho[(m_A^2-m_V^2+q^2)[\epsilon^*(\vec{p}_A,\lambda_A)\cdot p_V]\epsilon_\nu(\vec{p}_V,\lambda_V)\\ + (m_A^2-m_V^2-q^2)[\epsilon(\vec{p}_V,\lambda_V).p_A]\epsilon^*_\nu(\vec{p}_A,\lambda_A)]\Big].\end{aligned}$$

In this case[12] we computed with the vector at the source, produced using quark-smeared $\bar{\psi}\gamma^j\psi$ and a set of ten axial (actually T_1^{++}) operators at the sink.[13] In Fig. 6(a) we present the two transverse form factors for the ground-state axial meson, and in Fig. 6(b) we show their ratio. The amplitudes were each fitted with a form like Eq. (6), which unfortunately

[12]We could have used $\bar{\psi}\gamma^5\gamma^j\psi$ at the source to produce the axial meson; this operator at finite momentum also has overlap with the pseudoscalar state which severely limits its usefulness.

[13]$\gamma_i\gamma_5$, $\rho\times\nabla_{T1}$, $\rho_{(2)}\times\nabla_{T1}$, $a_1\times\mathbb{D}_{T1}$, $b_1\times\mathbb{B}_{T1}$ in both quark-smeared and unsmeared versions.

TABLE III. Results of the fit to lattice data using Eq. (6). We give the partial decay width computed using the fitted value of $\hat{V}(0)$ and physical phase space (where known). All errors are purely lattice statistical. Experimental partial decay widths are from [4,15].

Sink level	Suggested transition	$\hat{V}(0)$	β/MeV	λ/GeV^{-2}	$\Gamma_{\rm lat}$/keV	$\Gamma_{\rm expt}$/keV
0	$J/\psi \to \eta_c\gamma$	1.89(3)	513(7)	0 (fixed)	2.51(8)	1.85(29)
1	$\psi' \to \eta_c\gamma$	0.062(64)	530(110)	4(6)	0.4(8)	0.95(16)
						1.37(20)
3	$\psi'' \to \eta_c\gamma$	0.27(15)	367(55)	−1.25(30)	10(11)	···
5	$Y_{\rm hyb} \to \eta_c\gamma$	0.28(6)	250(200)	0 (fixed)	42(18)	···

is not as well constrained as in the scalar case, owing to the kinematic factors preventing a slightly timelike Q^2 point corresponding to $\vec{p}_i = \vec{p}_f = (000)$. The results of the fits are $a_t\hat{E}_1(0) = 0.23(3)$, $\beta_{E1} = 440(40)$ MeV, $\lambda_{E1} = 0.71(30)\,\text{GeV}^{-2}$ and $a_t\hat{M}_2(0) = -0.020(17)$, $\beta_{M2} = 450(50)$ MeV, $\lambda_{M2} = 5(6)\ \text{GeV}^{-2}$. This corresponds to a partial decay width of $\Gamma(\chi_{c1} \to J/\psi\gamma) = 270(70)$ keV which is in reasonable agreement with the PDG's average of 320(25) keV.

The ratio $\frac{M_2}{E_1}(Q^2)$, shown in Fig. 6(b), was fitted with various functional forms shown by the shaded bands yielding $\frac{M_2}{E_1}(0) = -0.20(6)$, where the error includes a crude estimate of the systematic error due to the uncertainty in the fitting form. The ratio of the extrapolated values from the separate fits to E_1, M_2 gives $\frac{M_2}{E_1}(0) = \frac{-0.020(17)}{0.23(3)} = -0.09(7)$. Clearly, without data points at smaller Q^2 or some certainty about the expected Q^2 dependence, we cannot constrain this any further and hence cannot make a particularly meaningful comparison with the PDG average $\frac{M_2(0)}{\sqrt{E_1(0)^2+M_2(0)^2}} = -0.002^{+0.008}_{-0.017}$.

Form factors for the transition from the first excited axial state χ'_{c1} down to the J/ψ are shown in Fig. 7, where multiple fit forms were used, all returning a $\chi^2/N_{\rm dof}$ close to 1. The estimates for the physical photon point thus obtained are $a_t\hat{E}_1(0) = 0.050(15)$ and $a_t\hat{M}_2(0) = -0.004(14)$, where again we include a crude systematic error estimate for the fit-form variation. The E_1 transition corresponds, for a χ'_{c1} at 4.1 GeV, to a partial decay width $\Gamma(\chi'_{c1} \to J/\psi\gamma) = 21(12)$ keV.

E. Tensor-vector transition

The transition between the lightest 2^{++} state and the lightest vector state was not considered in [2], as that study used only local fermion bilinears $[\bar{\psi}(x)\Gamma\psi(x)]$ to produce states—a spin-2 particle cannot be produced by any such operator. Here we use a set of six operators projected into T_2^{++} and E^{++} irreps at the sink.[14] The multipole decomposition for this transition takes the following form,

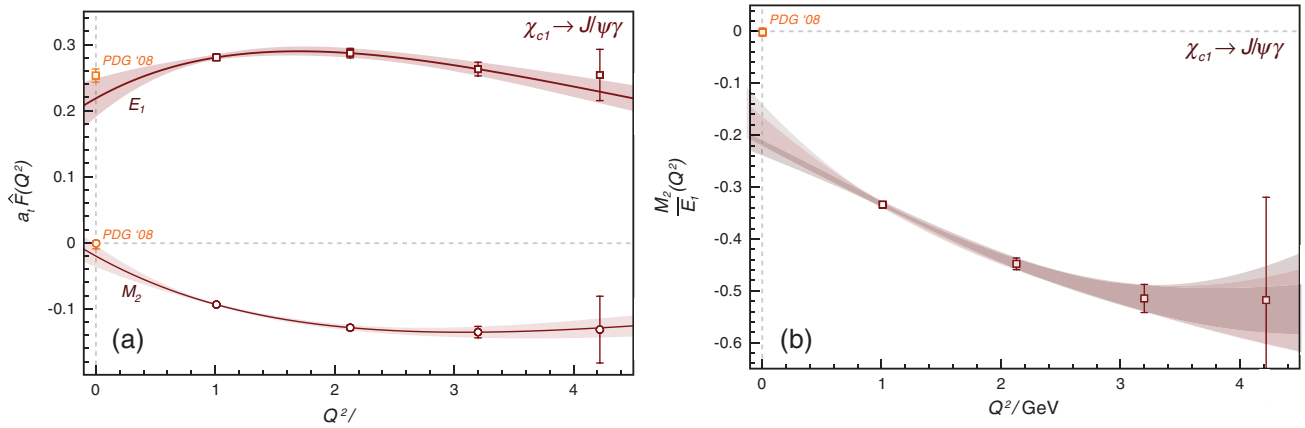

FIG. 6 (color online). (a) Electric dipole and magnetic quadrupole form factors for the transition $\chi_{c1} \to J/\psi\gamma$. We show the Q^2 dependence fitted with Eq. (6) and extrapolated to the physical photon point $Q^2 = 0$ for comparison with experimental data from [15]. The relative sign of E_1 to M_2 is relevant. (b) Ratio of magnetic quadrupole to electric dipole form factors. Colored bands represent fits with various fit functions.

[14] $\rho \times \nabla$, $\rho_{(2)} \times \nabla$, $b_1 \times \mathbb{B}$ in both quark-smeared and unsmeared versions.

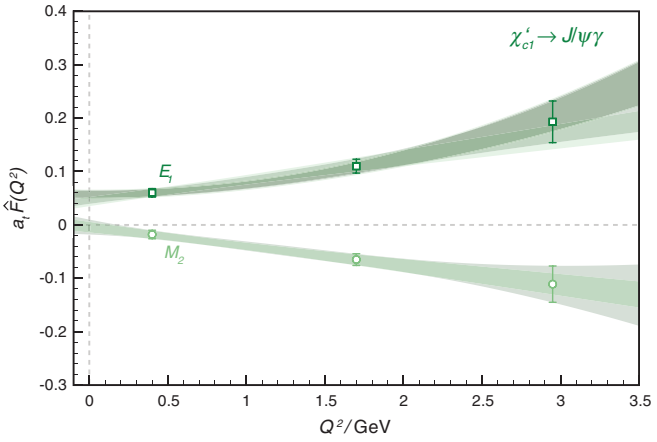

FIG. 7 (color online). Electric dipole and magnetic quadrupole form factors for the transition $\chi'_{c1} \to J/\psi\gamma$. We give the Q^2 dependence fitted with various forms shown by the colored bands. The relative sign of E_1 to M_2 is relevant.

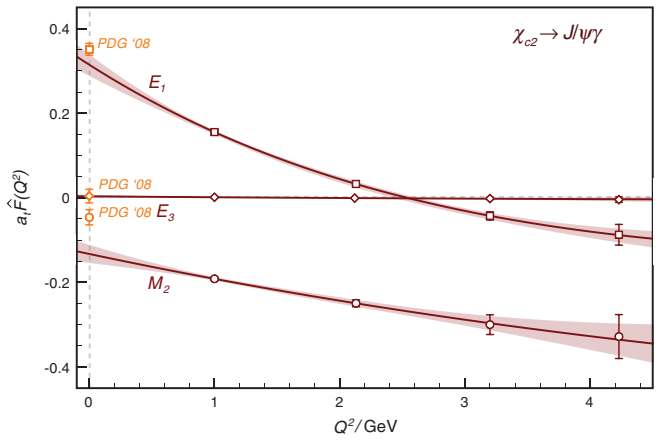

FIG. 8 (color online). Electric dipole, magnetic quadrupole, and electric octopole form factors for the transition $\chi_{c2} \to J/\psi\gamma$. We show the Q^2 dependencies fitted with Eq. (6) and extrapolated to the physical photon point $Q^2 = 0$ for comparison with experimental data from [15]. Relative signs are relevant.

$$
\begin{aligned}
&\langle V(\vec{p}_V, \lambda_V)|j^\mu(0)|T(\vec{p}_T, \lambda_T)\rangle \\
&= E_1(Q^2)\sqrt{\frac{3}{5}}\Big[-A^\mu + \frac{m_T}{\Omega}(\tilde{\omega} - m_V)B^\mu + \frac{m_T}{\Omega}(\tilde{\omega}D_T^\mu - m_T D_V^\mu) + \frac{m_T^2}{\Omega^2}(\tilde{\omega} - m_V)(-\tilde{\omega}F_T^\mu + m_T F_V^\mu)\Big] \\
&\quad + M_2(Q^2)\sqrt{\frac{1}{3}}\Big[A^\mu - \frac{m_T}{\Omega}(\tilde{\omega} + m_V)B^\mu - \frac{2m_T^2}{\Omega}C^\mu + \frac{m_T}{\Omega}(-\tilde{\omega}D_T^\mu + m_T D_V^\mu) \\
&\quad + \frac{m_T^2}{\Omega^2}((\tilde{\omega}^2 + \tilde{\omega}m_V - 2m_V^2)F_T^\mu + m_T(\tilde{\omega} - m_V)F_V^\mu)\Big] \\
&\quad + E_3(Q^2)\sqrt{\frac{1}{15}}\Big[-A^\mu + \frac{m_T}{\Omega}(\tilde{\omega} + 4m_V)B^\mu - \frac{5m_T^2}{2\Omega}C^\mu + \frac{m_T}{\Omega}(\tilde{\omega}D_T^\mu - m_T D_V^\mu) \\
&\quad + \frac{m_T^2}{\Omega^2}\Big(-\Big(\tilde{\omega}^2 + 4\tilde{\omega}m_V + \frac{5}{2}m_V^2\Big)F_T^\mu + m_T\Big(\frac{7}{2}\tilde{\omega} + 4m_V\Big)F_V^\mu\Big)\Big] \\
&\quad + C_1(Q^2)\sqrt{\frac{3}{5}}\frac{m_T}{\Omega\sqrt{q^2}}\Big[(m_V^2 - \tilde{\omega}m_T)D_T^\mu + (m_T^2 - \tilde{\omega}m_T)D_V^\mu - \frac{m_T}{\Omega}(\tilde{\omega} - m_V)((m_V^2 - \tilde{\omega}m_T)F_T^\mu + (m_T^2 - \tilde{\omega}m_T)F_V^\mu)\Big] \\
&\quad + C_3(Q^2)\sqrt{\frac{2}{5}}\frac{m_T}{\Omega\sqrt{q^2}}\Big[(m_V^2 - \tilde{\omega}m_T)D_T^\mu + (m_T^2 - \tilde{\omega}m_T)D_V^\mu - \frac{m_T}{\Omega}\Big(\tilde{\omega} + \frac{3}{2}m_V\Big)((m_V^2 - \tilde{\omega}m_T)F_T^\mu + (m_T^2 - \tilde{\omega}m_T)F_V^\mu)\Big].
\end{aligned}
\tag{7}
$$

Here $\Omega \equiv (p_T \cdot p_V)^2 - m_T^2 m_V^2$ and $\tilde{\omega} \equiv \frac{p_V \cdot p_T}{m_T}$ and

$$
\begin{aligned}
A^\mu &\equiv \epsilon^{\mu\nu}(\vec{p}_T, \lambda_T)\epsilon^*_\nu(\vec{p}_V, \lambda_V); \\
B^\mu &\equiv \epsilon^{\mu\nu}(\vec{p}_T, \lambda_T)p_\nu^V(\epsilon^*(\vec{p}_V, \lambda_V) \cdot p_T); \\
C^\mu &\equiv \epsilon^{*\mu}(\vec{p}_V, \lambda_V)(\epsilon^{\alpha\beta}(\vec{p}_T, \lambda_T)p_\alpha^V p_\beta^V); \\
D_T^\mu &\equiv p_T^\mu(\epsilon^{\alpha\beta}(\vec{p}_T, \lambda_T)\epsilon^*_\alpha(\vec{p}_V, \lambda_V)p_\beta^V); \\
D_V^\mu &\equiv p_V^\mu(\epsilon^{\alpha\beta}(\vec{p}_T, \lambda_T)\epsilon^*_\alpha(\vec{p}_V, \lambda_V)p_\beta^V); \\
F_T^\mu &\equiv p_T^\mu(\epsilon^{\alpha\beta}(\vec{p}_T, \lambda_T)p_\alpha^V p_\beta^V)(\epsilon^*(\vec{p}_V, \lambda_V) \cdot p_T); \\
F_V^\mu &\equiv p_V^\mu(\epsilon^{\alpha\beta}(\vec{p}_T, \lambda_T)p_\alpha^V p_\beta^V)(\epsilon^*(\vec{p}_V, \lambda_V) \cdot p_T).
\end{aligned}
$$

In order to have a constrained linear system for extraction of the five form factors, we are required to consider all five spin-2 helicities, which, with respect to the lattice cubic symmetry, are distributed in $T_2(3)$ and $E(2)$ irreps. Strictly speaking, these are independent irreps on the lattice and we should be careful about combining them; however, any lattice symmetry breaking must vanish as $a \to 0$, and in [1] we found that there were strong signals that the continuum rotational symmetry was restored to a good approximation already at this value of a. For example, for the ground states in the T_2, E channels, we have a high degree of mass

degeneracy, and the values of the overlaps (Z_{T_2}/Z_E) are compatible at the 1% level. Details of this analysis are in [1].

The extracted form factors and fits to the Q^2 dependence are shown in Fig. 8, where the expected hierarchy $|E_1(0)| > |M_2(0)| \gg |E_3(0)|$, to be discussed in Sec. IV B, is observed. The description of the lattice three-point correlators by the continuum decomposition, Eq. (7) (which does not take any account of T_2/E discretization differences), is excellent, with typically $\chi^2/N_{\rm dof} \sim 1$. As a simple systematic test of the degree to which T_2/E discretization differences could affect the determination of the form factors, we tried deliberately introducing such a difference by arbitrarily multiplying all E correlators by a factor. Even with a 10% increase in the magnitude of all E correlators, the form-factor values changed by less than the statistical error, while the $\chi^2/N_{\rm dof}$ increased to around 6. If we were to see such large χ^2 in our raw data (which we never do), we would not trust the results—we conclude that our form-factor extractions are not being strongly affected by T_2/E discretization differences.

The amplitudes at $Q^2 = 0$ correspond to a partial decay width of $\Gamma(\chi_{c2} \to J/\psi\gamma) = 380(50)$ keV to be compared with the PDG average of 406(31) keV. The electric dipole fit parameters are $\beta = 550(80)$ MeV and $\lambda = -0.39(1)$ GeV^{-2}. The fits yield values for the ratios of multipole amplitudes of $\frac{M_2(0)}{\sqrt{E_1(0)^2+M_2(0)^2+E_3(0)^2}} = -0.39(7)$ and $\frac{E_3(0)}{\sqrt{E_1(0)^2+M_2(0)^2+E_3(0)^2}} = 0.010(11)$; in the case of the first ratio, the value is considerably larger than the PDG average of $-0.13(5)$ but does appear to be of the correct sign.

We also extracted the $\chi'_{c2} \to J/\psi\gamma$ transition form factors[15] as presented in Fig. 9(a). The large value of E_3 might be surprising when compared to the ground-state result—a number of simple systematic tests were performed to investigate if this might come about through various lattice effects, with the result that we were unable to change the values outside statistical error bars by any reasonable adjustment. The amplitudes at $Q^2 = 0$ correspond to a partial decay width of 20(13) keV. In Fig. 9(b) we present the transition form factors for the next excited tensor state,[16] $\chi''_{c2} \to J/\psi\gamma$, where the hierarchy $|E_1(0)| > |M_2(0)| \gg |E_3(0)|$ appears to be restored and where we predict a partial decay width of 88(13) keV. In Sec. IV B we will propose a simple explanation for all these observations in the framework of a nonrelativistic quark model.

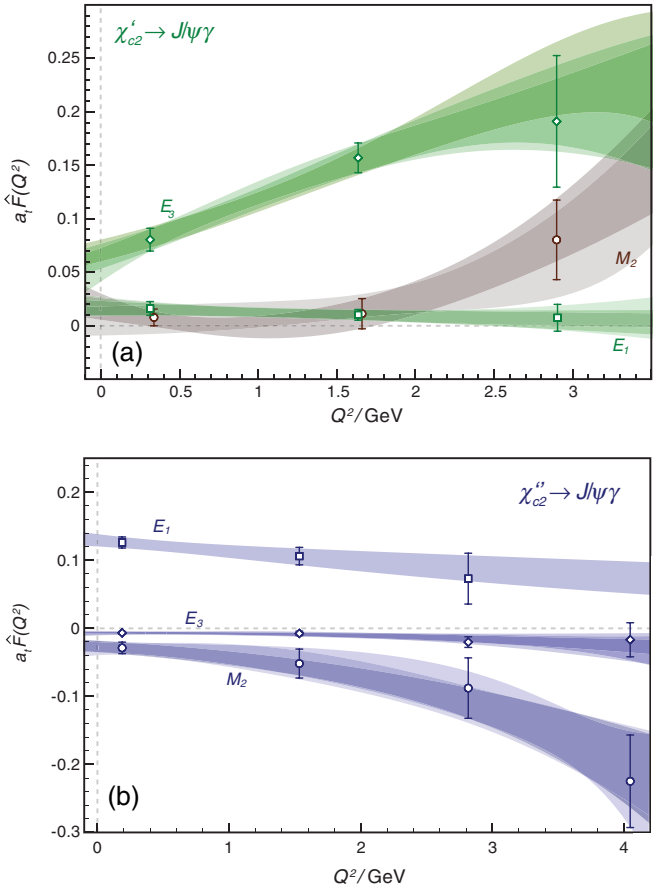

FIG. 9 (color online). (a) Electric dipole, magnetic quadrupole, and electric octopole form factors for the transition $\chi'_{c2} \to J/\psi\gamma$. Q^2 dependencies fitted with various fit forms are shown by the shaded bands. Relative signs are relevant. (b) Same as (a), but for $\chi''_{c2} \to J/\psi\gamma$.

F. Exotic transitions

Our principal focus here is on the exotic 1^{-+} state, η_{c1}, here[17] found to be at 4300(50) MeV. On a quenched lattice, provided we can eliminate the possibility that the lightest state in T_1^{-+} is part of a nonexotic 4^{-+} (see [12] for support of this elimination), we can be fairly certain that this state is a hybrid, having an excited gluonic field in addition to a charm-anticharm quark pair. This is in contrast to having a higher quark number Fock state which, since we lack light quarks altogether in this calculation, could only arise for states having mass near $4m_c$.[18] A charge-conjugation allowed decay of this meson would be $\eta_{c1} \to J/\psi\gamma$, having transverse magnetic dipole and electric quadrupole multipole contributions. The decomposition of the vector current matrix element between two

[15]We found a mass of 4115(28) MeV for the χ'_{c2}.
[16]We found a mass of 4165(30) MeV for the χ''_{c2}.
[17]But note our comments regarding the box size as a cause of systematic error.
[18]And in a quenched calculation, they would arise in a unitarity violating way [17].

nonidentical vector mesons takes the following form:

$$\begin{aligned}\langle V'(\vec{p}',\lambda')|j^\mu|V(\vec{p},\lambda)\rangle = -\left(\frac{m}{\sqrt{2\Omega}}\right)\Bigg[& M_1(Q^2)\Bigg(\epsilon^{\mu *}(\vec{p}',\lambda')(\epsilon(\vec{p},\lambda)\cdot p') + \frac{m'}{m}\epsilon^\mu(\vec{p},\lambda)(\epsilon^*(\vec{p}',\lambda')\cdot p) \\ & + (\epsilon(\vec{p},\lambda)\cdot p')(\epsilon^*(\vec{p}',\lambda')\cdot p)\left(\frac{q^\mu}{q^2}\left(\frac{m'}{m}-1\right)+\frac{q^2+\omega(m'-m)}{2\Omega}\Pi^\mu\right)\Bigg) \\ & + E_2(Q^2)\Bigg(\epsilon^{\mu *}(\vec{p}',\lambda')(\epsilon(\vec{p},\lambda)\cdot p') - \frac{m'}{m}\epsilon^\mu(\vec{p},\lambda)(\epsilon^*(\vec{p}',\lambda')\cdot p) + (\epsilon(\vec{p},\lambda)\cdot p')(\epsilon^*(\vec{p}',\lambda')\cdot p) \\ & \times\left(-\frac{q^\mu}{q^2}\left(\frac{m'}{m}+1\right)+\frac{q^2-\omega(m'+m)}{2\Omega}\Pi^\mu\right)\Bigg) \\ & + \frac{C_0(Q^2)}{\sqrt{q^2}}\left(\frac{q^2}{\sqrt{6}m}\right)\Pi^\mu\left((\epsilon^*(\vec{p}',\lambda')\cdot\epsilon(\vec{p},\lambda)) + \frac{m(\omega+m'-m)}{\Omega}(\epsilon(\vec{p},\lambda)\cdot p')(\epsilon^*(\vec{p}',\lambda')\cdot p)\right) \\ & + \frac{C_2(Q^2)}{\sqrt{q^2}}\left(\frac{q^2}{2\sqrt{3}m}\right)\Pi^\mu\left((\epsilon^*(\vec{p}',\lambda')\cdot\epsilon(\vec{p},\lambda)) - \frac{m(2m'+m-\omega)}{\Omega}(\epsilon(\vec{p},\lambda)\cdot p')(\epsilon^*(\vec{p}',\lambda')\cdot p)\right)\Bigg],\end{aligned}$$

where $\Pi^\mu = (p'+p)^\mu - \frac{m'^2-m^2}{q^2}(p'-p)^\mu$, $\Omega \equiv (p\cdot p')^2 - m^2m'^2$, and $\omega = \frac{m^2-m'^2+q^2}{2m}$.

We used a set of eight operators at the sink to produce the T_1^{-+} state.[19] Our results projected onto the ground state in T_1^{-+} are shown in Fig. 10—the lattice data are not fitted as a function of Q^2, as very little extrapolation is required to associate the point at $Q^2 = 0.06$ GeV with the real photon point. The value of $M_1(0)$ corresponds to a partial decay width $\Gamma(\eta_{c1} \to J/\psi\gamma) = 115(16)$ keV. Note that this is no different in scale from many measured conventional charmonium transitions.

If we also consider charge-conjugation symmetry violating decays (by coupling only to one quark), we have access to $1^{-(+)} \to 0^{-(+)}\gamma$, $1^{-(+)} \to 0^{+(+)}\gamma$. These results can be compared to models of hybrid bound-state structure, as we will do in the following section. Results are shown in Fig. 11.

Another exotic J^{PC} to which we have easy access is the 0^{+-} state which appears in the A_1^{+-} channel at 4465(65) MeV. We have computed a charge-conjugation symmetry violating decay of the lightest state with these quantum numbers to the conventional ground-state vector $1^{-(-)}$. This transition matrix element has the same decomposition as the vector-scalar in Eq. (5). We used a set of three operators[20] to create the $0^{+(-)}$ state; in Fig. 12 we show the electric dipole form factor for $0^{+(-)} \to 1^{-(-)}\gamma$.

G. Other assorted transitions

We also computed some C violating transitions which have allowed analogues in the light-quark sector,[21] $1^{+(+)} \to 0^{-(+)}\gamma$ and $2^{+(+)} \to 0^{-(+)}\gamma$. The first of these has a multipole decomposition identical to Eq. (5) while the second takes the form

$$\begin{aligned}&\langle P(\vec{p}_V)|j^\mu(0)|T(\vec{p}_T,\lambda)\rangle \\ &\quad = M_2(Q^2)\sqrt{2}\frac{m_T}{\Omega}\epsilon^{\mu\nu\rho\sigma}p_{T\rho}p_{P\sigma}\epsilon_{\nu\tau}(\vec{p}_T,\lambda)p_P^\tau.\end{aligned}$$

Results are shown in Fig. 13. A discussion in terms of nonrelativistic quark models follows in the next section.

IV. PHENOMENOLOGY

The results presented in the previous section can be compared with experimental measurements and, additionally, with the predictions of various models describing heavy-quark bound states. A rather successful approach to describing charmonium has emerged by considering heavy charm quarks to be moving nonrelativistically (or

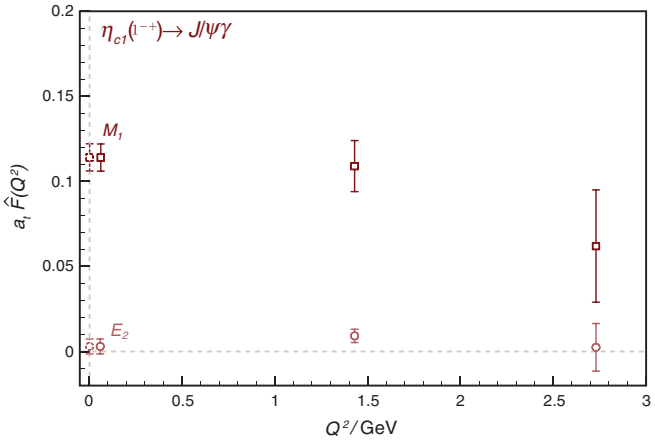

FIG. 10 (color online). Magnetic dipole and electric quadrupole form factors for the transition $\eta_{c1}(1^{-+}) \to J/\psi\gamma$. The point at $Q^2 = 0.06$ GeV is translated to the physical photon point $Q^2 = 0$.

[19] In the nomenclature of [1] they are smeared and unsmeared versions of $a_{0(2)} \times \nabla_{T1}$, $b_1 \times \nabla_{T1}$, $\rho \times \mathbb{B}_{T1}$, $\rho_{(2)} \times \mathbb{B}_{T1}$. The $\mathbb{B}$ operators induce an essential gluonic component through a factor proportional to $F^{\mu\nu}$ in the continuum limit; the ∇ operators reduce to covariant derivatives and hence have a factor A^μ.

[20] Quark-smeared $\bar{\psi}\gamma^0\psi$ and smeared and unsmeared $a_1 \times \mathbb{B}_{A1}$.

[21] Namely, $a_1^\pm \to \pi^\pm\gamma$ and $a_2^\pm \to \pi^\pm\gamma$.

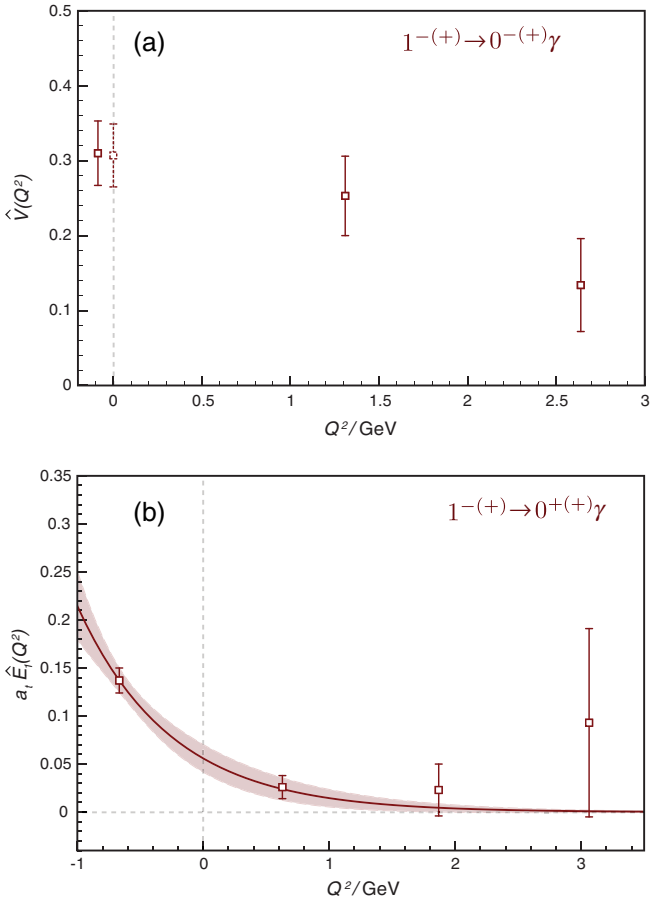

FIG. 11 (color online). (a) $1^{-(+)} \to 0^{-(+)}\gamma$ magnetic dipole transition. Linear interpolation using the two lowest-lying Q^2 points gives the value shown at $Q^2 = 0$. (b) $1^{-(+)} \to 0^{+(+)}\gamma$ electric dipole transition. The fit is with an exponential in Q^2.

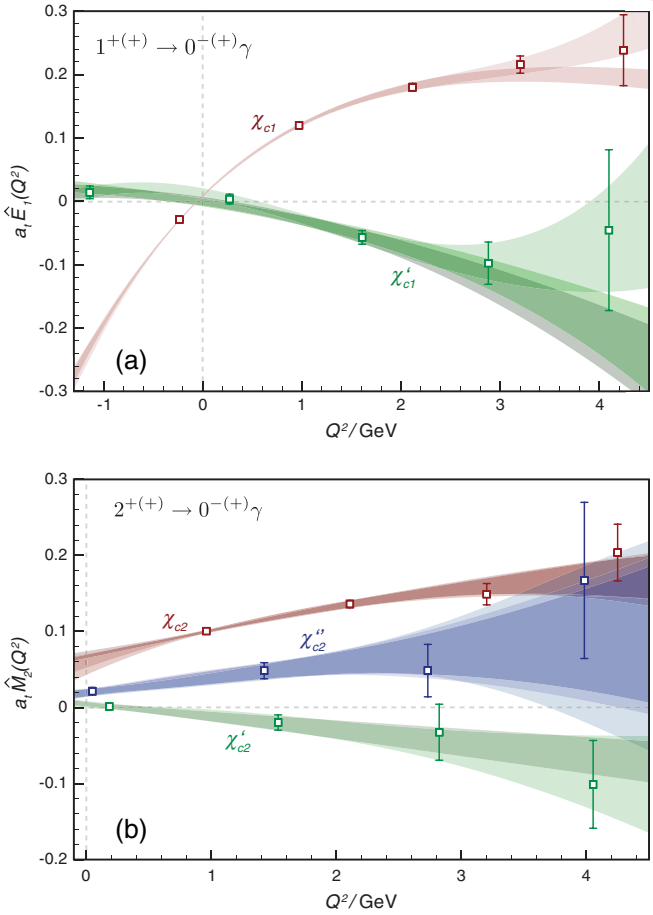

FIG. 13 (color online). (a) Electric dipole form factor for the transition $1^{+(+)} \to 0^{-(+)}\gamma$. (b) Magnetic quadrupole form factor for the transition $2^{+(+)} \to 0^{-(+)}\gamma$. Note that relative signs between states are not relevant.

nearly so) in a static potential motivated by QCD. These quark-potential models have been used to compute spectra, radiative transition rates, and, in many-body extensions of the theory, hadronic decay rates (e.g. [6,18,19]). In their simplest formulation, the gluonic field plays no dynamical role and one does not have exotic quantum numbered states with excited glue (hybrids). In order to consider such states one can construct models making specific assumptions about the nature of the gluonic field and its excitations, examples being the flux-tube model [20], "constituent" gluon models, and models based upon a many-body treatment of QCD in a physical gauge [21]. In what follows we will address to what extent our lattice QCD results inform these models.

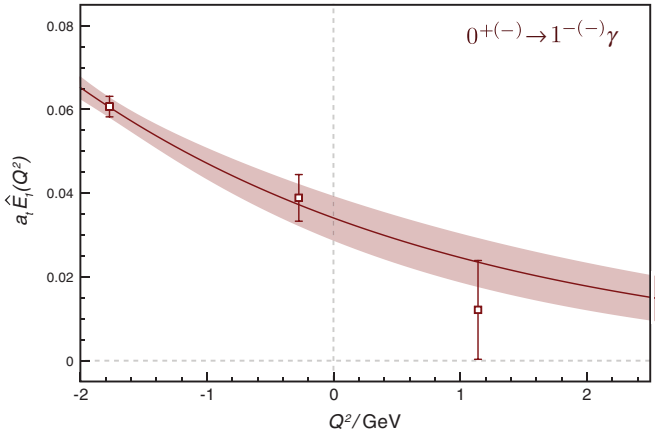

FIG. 12 (color online). Electric dipole form factor for the transition $0^{+(-)} \to 1^{-(-)}\gamma$. The fit is an exponential in Q^2.

First we should discuss the degree to which the approximations we have made in our computation introduce systematic error to our results.

A. Lattice systematics

This calculation has been performed within the quenched truncation—as such, one way to view it is as a calculation of a version of QCD having just one heavy flavor of quark, with the neglect of heavy flavor quark loops being justified by their large mass. In this regard this calculation is rather directly comparable to quark-potential models which in their simplest form also neglect

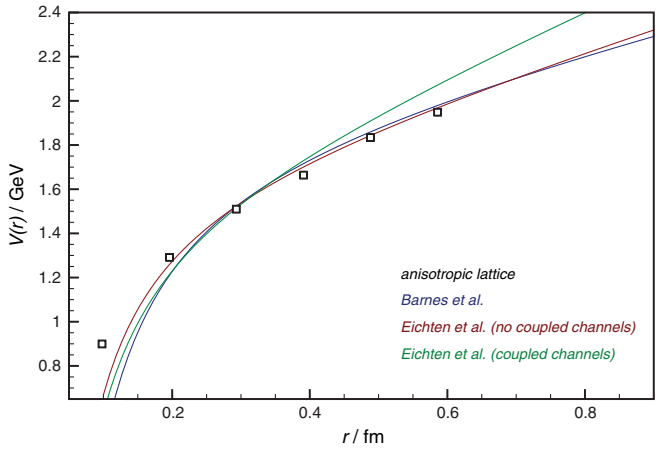

FIG. 14 (color online). Lattice static potential along with phenomenological potentials used in [7,18,34].

the effect of dynamical light quarks. We set the lattice scale in our calculation using the Sommer parameter which is itself related to the static quark potential and the charmonium spectrum, so here too the comparison is fairly direct. In Fig. 14 we show the static potential extracted on this lattice along with the phenomenological forms used in a selection of potential models.

Clearly, then our calculation does not include the effect of charmonium states coupling to multihadron states containing light quarks, e.g. $D\bar{D}$. There have been suggestions within extensions of quark-potential models that including such physics can have a considerable effect on the spectrum [5,6] and radiative transition rates [8] of charmonium. We will attempt to address this in the discussion to follow.

In terms of direct comparison with reality, in which there are three flavors of quarks lighter than charm, another failure introduced by the quenched approximation is the incorrect running of the strong coupling due to the beta function containing the wrong number of quark degrees of freedom. We expect this to show up in terms of inconsistent scale setting—something that has been observed previously [22].

Our calculation has been performed at only one value of the lattice spacing; as is well known, one expects there to be systematic shifts in quantities, owing to the lattice discretization that goes away as one approaches the continuum. These are suggested to be particularly serious for the discretization of heavy quarks. At a single lattice spacing we cannot accurately estimate the size of such effects, although our use of the improved clover action and an anisotropic lattice[22] should help a great deal in the reduction. We present in Appendix B a limited study of improving the vector current insertion in the manner described in [23]. In general, the improvement effects are not large, suggesting that scaling to the continuum should not overwrite our results.

In the spectrum calculations using the same action on the same lattices [1,12], the possibility that the spatial volume is too small to comfortably house highly excited states was raised.

One way to reduce the systematic error introduced by extrapolating from finite Q^2 to $Q^2 = 0$ would be to consider utilizing twisted boundary conditions on the propagator inversions to get momenta and hence Q^2 values rather close to $Q^2 = 0$—this has proven to be successful in form-factor computations [24].

Modulo the caveats that we have raised, we remain convinced that the results we present likely represent a faithful description of the pattern of physics of radiative transitions in charmonium, including the properties of gluonic hybrids. Most importantly, we have clearly demonstrated that the technology of projecting three-point functions using ideal operator eigenvectors obtained in two-point function calculations works well in giving us access to excited-state transitions. All the possible sources of systematic error can be addressed in future calculations using a set of sufficiently large dynamical lattices of various lattice spacings.

B. Conventional-state transitions and the quark-potential model

Reference [12] used information extracted from two-point functions to identify excited charmonium states found in a lattice calculation with the corresponding states expected in the quark model. The transition form factors can also be compared to calculations in quark-potential models. Our quenched lattice calculations offer a rather direct comparison with these potential models: in both cases loops of mesons containing light quarks have been ignored. As discussed in Refs. [2,25], the results of quark models are sensitive to approximations, such as the choice of frame, which are not an issue in lattice calculations—we will not discuss these further here. In the following, for simplicity, we use harmonic oscillator wave functions and consider the rest frame of the initial meson.

Within the simplest nonrelativistic model of a meson emitting a photon of momentum $\vec{q}$, we find the following transition form factors for nonradially excited states undergoing a change of orbital angular momentum of one unit:

$$E_1(|\vec{q}|^2) \propto \left[1 + r\frac{|\vec{q}|^2}{4\beta^2}\right]\exp\left(-\frac{|\vec{q}|^2}{16\beta^2}\right) \tag{8}$$

where β is the harmonic oscillator wave-function parameter. Here the r values follow from the coupling of quark spin and orbital angular momentum as[23]

[22]Some comparison of the clover action with the domain wall action on these lattices is given in [1].

[23]Note that a typographical error in [2] is corrected here.

$$
\begin{aligned}
r &= 1, && \chi_{c0}(^3P_0) \to J/\psi(^3S_1)\gamma, \\
r &= 1/2, && \chi_{c1}(^3P_1) \to J/\psi(^3S_1)\gamma, \\
r &= -1/2, && \chi_{c2}(^3P_2) \to J/\psi(^3S_1)\gamma, \\
r &= 0, && h_c(^1P_1) \to \eta_c(^1S_0)\gamma.
\end{aligned}
$$

Transforming from $|\vec{q}|^2$ to the invariant virtuality of the photon (Q^2) in the rest frame of the decaying meson, this corresponds to

$$E_1(Q^2) \propto \left[1 + r\frac{Q^2}{4\beta^2}\frac{1+\Delta}{1+r\delta}\right]\exp\left(-\frac{Q^2}{16\beta^2}(1+\Delta)\right) \tag{9}$$

with $\Delta \equiv \frac{m_f^2 - m_i^2}{2m_i^2}$ and $\delta \equiv \frac{(m_f^2-m_i^2)^2}{16m_i^2\beta^2}$. Note that this is of the general form given in Eq. (6).

In the same model, we have for transitions involving both a change in orbital angular momentum and a quark spin-flip, the expression

$$E_1(|\vec{q}|^2) \propto \frac{|\vec{q}|^2}{\beta^2}\exp\left(-\frac{|\vec{q}|^2}{16\beta^2}\right). \tag{10}$$

This applies to the charge-conjugation forbidden decays $1^{+(+)}(^3P_1) \to 0^{-(+)}(^1S_0)\gamma$ and $1^{+(-)}(^1P_1) \to 1^{-(-)}(^3S_1)\gamma$. In addition, this same form is predicted for the M_2 form factor in the transitions $\chi_{c1,2}(^3P_{1,2}) \to J/\psi(^3S_1)\gamma$ and the charge-conjugation forbidden $2^{+(+)}(^3P_2) \to 0^{-(+)}(^1S_0)\gamma$ and $1^{+(-)}(^1P_1) \to 1^{-(-)}(^3S_1)\gamma$. In terms of Q^2 this gives

$$E_1(Q^2) \propto \left[\delta + \frac{Q^2}{4\beta^2}(1+\Delta)\right]\exp\left(-\frac{Q^2}{16\beta^2}(1+\Delta)\right), \tag{11}$$

which we note is also of the form of Eq. (6).

Within this model we find that $E_3(Q^2) = 0$ for $\chi_{c2}(^3P_2) \to J/\psi(^3S_1)\gamma$. In fact, this result follows from the general assumption of a *single quark transition* [26] and does not depend critically upon the details of the model. For a transition $J \to J'$ (where J and J' are, respectively, the initial and final meson spins) the allowed k (for E_k or M_k depending on k and the parity change) are, in general, $|J - J'| \le k \le J + J'$. However, if only a single quark is involved in the transition, there is a further restriction on the values allowed. If the interacting quark in the initial (final) meson has total angular momentum j (j'), then $|j - j'| \le k \le j + j'$. Hence, in general, for an $n^3P_2 \to n'^3S_1$ transition the allowed k are $k = 1, 2, 3$. However, in the single quark transition assumption we have $j = 3/2 \to j' = 1/2$ and k is restricted to $k = 1, 2$. Note that it *is* possible to have $E_3 \neq 0$ if the tensor meson is a $^3F_2$ ($j' = 5/2$) state, in which case $k = 2, 3$ and $E_1 = 0$. It is also possible to have $E_3 \neq 0$ in transitions involving hybrid, multiquark, or molecular mesons where there are other degrees of freedom able to carry some angular momentum.

1. ψ-η_c transitions

Our result for $\Gamma(J/\psi \to \eta_c\gamma)$ is in reasonable agreement with the new experimental value from CLEO-c [4], the potential model calculations of [18,27], the potential nonrelativistic QCD result of [28], and the QCD sum-rule estimate of [29]. Similarly, our result for the "hindered" M_1 transition $\Gamma(\psi' \to \eta_c\gamma)$ is consistent with the experimental values in [4,15] and Eichten *et al.* [27], but significantly smaller than the values in Ref. [18] which depend sensitively on the overlap of orthogonal wave functions with a small recoil factor breaking the orthogonality.

Li and Zhao [8] study the possibility of hadronic loop contributions in J/ψ and ψ' radiative decays to η_c and η_c'. They find that the addition of loop contributions involving pairs of D and D^* mesons can bring the model values from Ref. [18] into line with experiment. Most significantly, they find large loop contributions, of order 10 keV, to the $\psi' \to \eta_c\gamma$ transition. A cancellation between the quark-model contribution of order 10 keV (from Ref. [18]) and these loop contributions results in a small transition width of $\sim$1 keV. This appears to present a problem with respect to our result, which being quenched does not include loop contributions, since there is no room for a large loop contribution when our $\Gamma(\psi' \to \eta_c\gamma)$ is compared to the experimental value. This might indicate that the loop contributions of Ref. [8] are overestimated, and we have identified one possible source for this in the coupling $g_{D^*D\gamma}$ used. The partial decay width $\Gamma(D^{*0} \to D^0\gamma) \sim$ 800 keV assumed in Ref. [8] appears to be rather large for an M_1 radiative transition and, with the branching ratio from the PDG [15], implies a D^{*0} total width of 2.1 MeV which is at the upper limit allowed by the PDG. For comparison, Close and Swanson [30], using a nonrelativistic quark model, predict $\Gamma(D^{*0} \to D^0\gamma) = 32$ keV. The corresponding decrease in the loop amplitudes would remove the problem in comparison with our result. In addition, there are considerable uncertainties arising from the estimated hadronic coupling constants in the loop contributions which are not discussed in Ref. [8]. These uncertainties may be particularly important because of the delicate nature of the cancellation.

We have also been able to extract a signal for the $\psi'' \to \eta_c\gamma$, which in the standard interpretation of the ψ'' would be a $1^3D_1 \to {}^1S_0$ transition. In a harmonic oscillator wave-function basis the form factor has the same leading $|\vec{q}|^3$ behavior as $2^3S_1 \to {}^1S_0\gamma$, indicating that it should suffer hindered suppression just like the $\psi' \to \eta_c\gamma$ relative to $J/\psi \to \eta_c\gamma$. The lattice data for the amplitude appear to be in line with this, within a large statistical uncertainty. Discussion of the next excited vector state will follow in Sec. IV C.

2. χ-ψ transitions

The $\chi_{cJ} \to J/\psi\gamma$ partial widths we obtain are dominated by the electric dipole component and compare favor-

ably with the experimental values. The largest discrepancy is in the statistically precise χ_{c0} transition. The lattice systematic errors discussed above may be to blame for this; without further calculation we cannot determine this definitively, but we note that [7] found that approximately "unquenching" the quark model for this transition did not induce a large change in the rate. In Appendix B we consider the effect of using an improved vector current, and we find that the $\chi_{c0} \to J/\psi\gamma$ transition is one case where a statistically significant change with respect to the local current does occur. This might indicate that this transition is particularly sensitive to scaling in the lattice spacing.

The fitted values of β in Eq. (6) are in rough agreement for all of $\chi_{c0,1,2}$, as one might expect for states that in the potential model differ only by small spin-orbit effects. The fitted values of λ deviate somewhat from the expected quark-model ratio $1{:}\frac{1}{2}{:}-\frac{1}{2}$ for $\chi_{c0,1,2}$, being 1:0.62(26):$-$0.34(2). Given the approximations and frame dependence inherent in the quark model, even such rough agreement is surprising.

In the $\chi_{c1,2} \to J/\psi\gamma$ transitions, the hierarchy of multipoles expected in the quark model [$|E_1(0)| > |M_2(0)| \gg |E_3(0)|$] is observed. The precise degree of suppression of M_2 compared with E_1 is not easy to compute in nonrelativistic quark-potential models. However, the single quark transition assumption predicts that $E_3(Q^2) = 0$, independent of the frame and details of the potential, and that the lattice data do agree with this. Our extracted values of $M_2(0)$ or the ratio $M_2(0)/E_1(0)$ all depend upon theoretically undetermined extrapolation in Q^2, and so the apparent disagreement with the very small values found in experiment is not yet overly concerning.

The electric dipole couplings for $\psi' \to \chi_{c0}\gamma$ and $\psi'' \to \chi_{c0}\gamma$ are, within reasonably large statistical errors, in agreement with experimental values and with the "GI" values tabulated in [18].[24] The estimates of D-meson loop effects from [7] are comparable to the level of our statistical uncertainty.

For the transition $\chi'_{c1} \to J/\psi\gamma$ we extract a partial width of 21(12) keV which is in reasonable agreement with the quark-model estimates of [18], being 14 or 71 keV depending upon model details. Since in our study this state has a likely interpretation as the 2^3P_1 state of the quark model, without any $D\bar{D}^*$ effects included, this can act as a benchmark for models that consider the experimental $X(3872)$ state as being 1^{++}.

The large $E_3(0)$ in the lattice calculation of the $\chi'_{c2} \to J/\psi\gamma$ transition is in stark disagreement with the general result that $E_3 = 0$ for a ${}^3P_2 \to {}^3S_1$ transition. As discussed above, this does not appear to be a lattice artifact and so another interpretation must be found. Possible explanations include that the χ'_{c2} state is a hybrid where the gluonic field carries spin, but here we concentrate on the most conservative interpretation, that χ'_{c2} is a conventional ${}^3F_2$ state.

An F-wave tensor state (${}^3F_2$) is expected to have $E_1(Q^2) = 0$, in general, from the single quark transition assumptions outlined earlier. In addition, a quark-model calculation shows that $M_2(0)$ is highly suppressed:

$$M_2(|\vec{q}|^2) \propto \frac{|\vec{q}|^4}{\beta^4} \exp\left(-\frac{|\vec{q}|^2}{16\beta^2}\right),$$

whereas E_3 is less suppressed:

$$E_3(|\vec{q}|^2) \propto \frac{|\vec{q}|^2}{\beta^2} \exp\left(-\frac{|\vec{q}|^2}{16\beta^2}\right),$$

with the same leading $|\vec{q}|^2$ dependence as the M_2 form factor in a ${}^3P_2 \to {}^3S_1$ transition [Eq. (11)]. This pattern that $|E_3(0)| > |M_2(0)| \gg |E_1(0)|$ is consistent with the lattice results for this $\chi'_{c2} \to J/\psi\gamma$ transition. These lattice results support the interpretation of this χ'_{c2} as the lightest ${}^3F_2$ state having a partial decay width to $J/\psi\gamma$ of 20(13) keV. We are unaware of any model calculations of this transition rate.

The $\chi''_{c2} \to J/\psi\gamma$ transition appears to have reverted to the $|E_1(0)| > |M_2(0)| \gg |E_3(0)|$ hierarchy expected for a ${}^3P_2$ state, and we propose that this state is the 2^3P_2. There is of course the possibility that the P and F states are mixed, but this mixing cannot be anything like maximal mixing given that a large E_3 only appears in one case and a large E_1 only appears in the other case. Within a nonrelativistic quark model, the ${}^3P_2$ and ${}^3F_2$ states can mix via any tensor potential in the Hamiltonian. However, in most models this term is suppressed by the inverse charm mass squared and so is small. The tensor term, like the hyperfine interaction, is a short-distance effect and so may not be reliable in these quenched lattice calculations. Because this term is suppressed anyway, the errors introduced from this should be small. Another possible source of mixing which we lack in the quenched theory comes through $D\bar{D}$ meson loops—such effects are discussed in [5,31].

The partial decay width $\Gamma(\chi''_{c2} \to J/\psi\gamma)$ extracted from the lattice data is 88(13) keV, which is comparable with the 53 or 81 keV computed by [18]. We note that the interpretation of excited states in this channel as F and P waves was hinted at in the two-point function analysis of [12], where states compatible with being ${}^3F_2$ and 2^3P_2 were found to be nearly degenerate. Within the quark-potential models used in [18], the F wave state is expected to be 60–100 MeV heavier than the P wave. The approximate degeneracy we found may be an artifact of "squeezing" these spatially larger states into a 1.2 fm box.

A discussion of the excited χ_{c2} states is timely, given the observation of a candidate state at 3929(5) MeV by Belle in $\gamma\gamma \to D\bar{D}$ which has been associated with the 2^3P_2 state

[24]But note the considerable dependence on the details of the quark model in that paper's "NR" results.

[32]. We lack reliable theoretical estimates of the $\gamma\gamma$ widths of $^3F_2$ and 2^3P_2 states—this calls for an extension of the work done in [33] to consider excited states which could use operator projection technology very similar to that discussed in this paper. We note here that an optimist viewing Fig. 2 of [32] might hope that the statistically insignificant excess at 4080 MeV could, with increased statistics, become a signal for the other state in the $2^3P_2/1^3F_2$ pair.

The $J^{+(+)} \to 0^{-(+)}\gamma$ transitions shown in Fig. 13 are consistent with the quark-model predictions. The electric dipole amplitudes in $1^{+(+)} \to 0^{-(+)}\gamma$ are much smaller than other electric dipole amplitudes since they involve both $\Delta L = 1$ and a spin-flip. For the magnetic quadrupole amplitudes in $2^{+(+)} \to 0^{-(+)}\gamma$, the $^3P_2$ amplitude behaves like Eq. (10) while the $^3F_2$ amplitude is suppressed by a two more powers of $|\vec{q}|$ which suggests yet again the assignment $\chi_{c2} = 1^3P_2$, $\chi'_{c2} \approx 1^3F_2$, and $\chi''_{c2} \approx 2^3P_2$.

C. Exotic and crypto-exotic transitions

The only charge-conjugation allowed transition involving an exotic we compute, $\eta_{c1} \to J/\psi\gamma$, has a rather large partial decay width 115(16) MeV which is dominantly through a magnetic dipole transition. Even accounting for the large phase space, this is very large on the usual scale of magnetic dipole transitions. Conventional $c\bar{c}$ states can only have magnetic dipole transitions if there is a quark spin-flip, and this is suppressed by the large charm-quark mass. In a hybrid meson the extra gluonic degree of freedom allows an M_1 transition *without spin-flip*. This can be seen explicitly within the flux-tube model, where in an M_1 transition between a conventional $L = 0$ meson and a hybrid meson, the tube absorbs the angular momentum.[25]

The two-point function analysis of [12] suggested that the excited vector state we have called $Y_{\rm hyb}$ (having mass around 4.4 GeV) is a crypto-exotic hybrid meson, having nonexotic $J^{PC} = 1^{--}$ but internally an excited gluonic field. That analysis preferred the quarks to be in a spin singlet in this state. In that case we would expect a large non-spin-flip M_1 transition $Y \to \eta_c\gamma$ which is precisely what is seen in our lattice data. Here $\Gamma(Y \to \eta_c\gamma) = 42(18)$ keV, which is considerably larger than any other vector-to-pseudoscalar transition. Within the flux-tube model, the nonexotic $Y(1^{--}_{\rm hyb})$ and the exotic $\eta_{c1}(1^{-+}_{\rm hyb})$ (which we find at a mass ~4.3 GeV) differ only in being quark spin singlets and triplets, respectively, and $\Gamma(Y \to \eta_c\gamma) \approx \Gamma(\eta_{c1} \to J/\psi\gamma)$. The lattice data do not strongly disagree with this. It would be very interesting to see analogous calculations in other models of excited glue to see if this is a general result or one peculiar to the flux-tube model.

[25]Details are presented in the unpublished D.Phil. thesis of J. J. D. where the following partial widths were obtained: $\Gamma(\eta_{c1} \to J/\psi\gamma) \approx \Gamma(Y_{\rm hyb} \to \eta_c\gamma) \approx 30 \to 60$ keV.

We also consider charge-conjugation violating electric dipole transitions involving exotic mesons, $1^{-(+)} \to 0^{+(+)}\gamma$ and $0^{+(-)} \to 1^{-(-)}\gamma$, where for both we found nonzero signals. Roughly speaking, one can gauge the cost of exciting the gluonic field versus exciting conventional orbital angular momentum by comparing the electric dipole transitions $1^{-(+)} \leftrightarrow 0^{+(+)}$ having $E_1(0) = 0.06(1)$, and $1^{-(-)} \leftrightarrow 0^{+(+)}$ having $E_1(0) = 0.127(2)$. These numbers are clearly of the same order, a result that is also true in the flux-tube model [10,11]—whether this is true in other models has not yet, to our knowledge, been tested. The transition $0^{+(-)} \to 1^{-(-)}$ where $E_1(0) \sim 0.04(1)$ suggests that $L_{q\bar{q}} = 0$ transitions to exotic hybrids are also unsuppressed.

Further evidence for the quark spin-triplet nature of the $\eta_{c1}(1^{-+}_{\rm hyb})$ and the quark spin-singlet nature of the $Y(1^{--}_{\rm hyb})$ comes from the fact that $E_1(0)$ for $1^{-(+)} \to 0^{+(+)}\gamma$ is 0.06(1) while for $1^{-(-)}_{\rm hyb} \to 0^{+(+)}\gamma$ it is consistent with zero. The first of these then is $(S_{q\bar{q}} = 1) \to (S_{q\bar{q}} = 1)$ while the second requires a spin-flip, expected to be suppressed by the heavy-quark mass. Note that the magnetic dipole transition $1^{-(+)} \to 0^{-(+)}\gamma$ in Fig. 11 is at the scale of other hindered M_1 transitions, consistent with requiring both gluonic excitation and quark spin-flip. We note that the spin-singlet nature of our Y state does not make it a good candidate for the experimental $Y(4260)$ state whose potentially large decay rate into $\pi\pi J/\psi$ would tend to suggest dominance of the spin triplet.

Here we briefly comment that if this heavy-quark hybrid physics is any guide to the behavior of light-quark hybrid systems, we should expect the GlueX experiment to copiously photoproduce hybrid mesons off the meson cloud around a baryonic target.

V. CONCLUSIONS

We have demonstrated that the ideal excited-state operators within a basis of operators can be used to successfully extract excited-state transitions from three-point correlators. Using this technique we have carried out an extensive survey of radiative transitions in charmonium with detailed consideration of the phenomenology suggested by the results.

Notably we have performed the first lattice QCD calculation of the exotic η_{c1} radiative decay and found a large $\Gamma(\eta_{c1} \to J/\psi\gamma) = 115(16)$ keV. We found statistically significant electric dipole and magnetic quadrupole form factors in $\chi_{c2} \to J/\psi\gamma$, calculated for the first time in this framework, and have studied excited $\chi_{c1,2}$ transitions. Our results for the excited χ_{c2} states suggest that there could be a radially excited 2^3P_2 state and a 1^3F_2 state rather close in mass. This signal followed from a clear observation of dominance of E_1 over E_3 in one case and E_3 over E_1 in the other and matches the general expectations of potential

models. This is relevant given the recent observation of a candidate 2^{++} excited state in $\gamma\gamma \to D\bar{D}$ [32].

Our calculation of magnetic dipole transition widths, such as $\psi \to \eta_c \gamma$ and hindered excited-state transitions, reflect the expected suppression of the excited-state transitions. We note that, modulo lattice systematic effects which can be reduced, our method is not troubled by the uncontrolled approximations and model dependence inherent in model calculations of such suppressed transitions. In light of this we were able to make statements regarding the possible influence of closed channel D-meson loops on the hindered transitions, determining that they cannot be as large as suggested in certain studies. We identified a putative nonexotic hybrid state having a large magnetic dipole transition amplitude to η_c—the possibility that this reflects the non-spin-flip magnetic dipole excitation allowed within the flux-tube model (and likely within other models having more than $c\bar{c}$ content) was raised.

While the current numerical results may be affected by lattice systematic errors, future calculations using the now proven methodology can address these shortcomings by using dynamical lattices of sufficient size and a number of different lattice spacings. At some point after the introduction of dynamical lattices, the difficulty of dealing with resonant states embedded in a multimeson continuum will have to be addressed.

We have demonstrated that our results are in agreement with general predictions of quark-potential models but we are able to go beyond this to make statements about states in which there is an excited gluonic field. These results are appropriate for comparison with models proposing particular forms for the gluonic excitation.

The great advantage of this development within lattice QCD, as compared to models relying upon the nonrelativistic motion of quarks, is its immediate applicability to the light-quark systems. Future efforts will consider photocouplings of light-quark mesons, and, in particular, exotics, as these are of central importance in the production rates for the GlueX project. If the large couplings we find for the 1^{-+} state with heavy quarks persist into the light-quark sector, this will confirm the intuition and model results used to motivate the GlueX production process.

ACKNOWLEDGMENTS

We acknowledge fruitful discussions with our colleagues David Richards and Nilmani Mathur. We thank Qiang Zhao for his communications regarding his research on hadron loops, and Matt Shepherd and Ryan Mitchell for their communications regarding CLEO-c. This work was supported by DOE Contract No. DE-AC05-06OR23177, under which Jefferson Science Associates, LLC, operates Jefferson Laboratory. Computations were performed on clusters at Jefferson Laboratory as part of the USQCD Collaboration.

APPENDIX A: DERIVATIVE OPERATORS AT ZERO AND NONZERO MOMENTUM

In this appendix we give a few details of the spin structure we deal with when considering two- and three-point correlators. We take the example of the T_1^{--} vector operators considered at $\vec{p} = (000)$ and $\vec{p} = (100)$. Using the decompositions in Appendix A of [1], we find that at zero momentum all the operators we have used have the following behavior in the continuum limit,

$$\langle 1^{--}(\vec{p} = \vec{0}, \lambda)|\mathcal{O}_i|0\rangle \propto \epsilon_i^*(\vec{0}, \lambda), \tag{A1}$$

and there are no nonzero overlaps onto particles of any other J^{PC} (except those lattice artifacts that appear suppressed by powers of a). The three-point correlator then involves a sum $\sum_\lambda \epsilon_i^*(\vec{0}, \lambda)\epsilon_j(\vec{0}, \lambda) = -g_{ij}$.

At nonzero momentum things are not so simple; with one unit of lattice momentum [e.g. $\vec{p} = (100)$] we have the following nonzero overlaps in the continuum limit,

$$\begin{aligned}
&\langle 1^{--}(\vec{p}, \lambda)|\mathcal{O}_i|0\rangle \sim \epsilon_i^*(\vec{p}, \lambda),\ p_j\epsilon_j^*(\vec{p}, \lambda)p_i,\\
&\langle 1^{+-}(\vec{p}, \lambda)|\mathcal{O}_i|0\rangle \sim \epsilon_{ijk}\epsilon_j^*(\vec{p}, \lambda)p_k,\\
&\langle 0^{+-}(\vec{p})|\mathcal{O}_i|0\rangle \sim p_i,\\
&\langle 2^{+-}(\vec{p})|\mathcal{O}_i|0\rangle \sim p_j\epsilon_{ij}^*(\vec{p}, \lambda),\ p_i\epsilon_{00}^*(\vec{p}, \lambda).
\end{aligned} \tag{A2}$$

These forms are derived following the decompositions given in Appendix A of [1].[26]

So here we have additional contributions from $(0, 1, 2)^{+-}$ particles—the $(0, 2)^{+-}$ contributions we can neglect, as these exotic states are very heavy, but the 1^{+-} we must worry about. We can see the entry of such particles in the two-point function spectral analysis; in Fig. 15 we show the spectrum at $\vec{p} = (100)$ with either $i = x$, where 1^{+-} does not contribute, or with $i = y, z$, where 1^{+-} can contribute. Also shown are the T_1^{--} and T_1^{+-} spectra extracted at $\vec{p} = (000)$ extrapolated to $\vec{p} = (100)$ using the continuum dispersion relation $E = \sqrt{m^2 + |\vec{p}|^2}$. We see the entry of the lightest 1^{+-} state into the $T_1^{--}(\vec{p} = (100))$ spectrum in the case $i = y, z$ but not in the case $i = x$ as expected. We can explicitly exclude this state from our three-point analysis by not projecting onto the eigenvector belonging to this level. In the results presented in Figs. 4 and 5 we separately consider the cases $i = x$ and $i = y, z$ shown by the triangles and the circles. Note that we did not simply rely upon energy matching to determine the levels—a more precise mapping between $\vec{p} = (000)$ levels and $\vec{p} = (100)$ comes from considering the overlaps, Z. As a concrete example consider the matrix elements $\langle 1^{--}(\vec{p}, \lambda)|\bar{\psi}\gamma_i\psi|0\rangle = Z\epsilon_i^*(\vec{p}, \lambda)$ where Z is proportional to the vector decay constant and where, for unsmeared quark fields in the continuum limit, Z should be independent of momentum $\vec{p}$. As can be clearly seen in Table IV,

[26]Correcting some minor typographical errors therein.

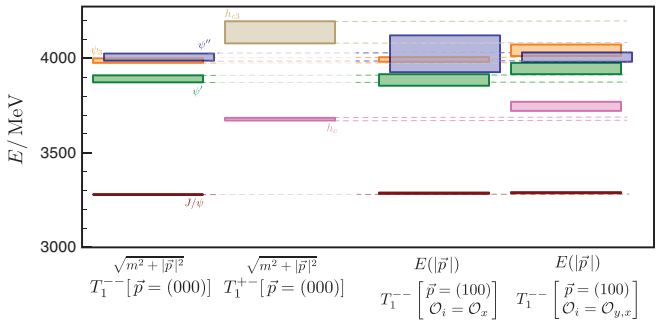

FIG. 15 (color online). Low-lying spectrum extracted from two-point correlators. The state assignment (color coding) follows from the consideration of the overlap factor as described in the text.

TABLE IV. Z values in $\langle 1^{--}(\vec{p},\lambda)|\bar{\psi}\gamma_i\psi|0\rangle = Z\epsilon_i^*(\vec{p},\lambda)$. The state proposed to be J/ψ is in bold, and the state proposed to be ψ' is in italics.

Level	$\vec{p}=(000)$	$\vec{p}=(100)$ $\mathcal{O}_i=\mathcal{O}_x$	$\vec{p}=(100)$ $\mathcal{O}_i=\mathcal{O}_{y,z}$
0	**0.163(1)**	**0.173(1)**	**0.166(1)**
1	*0.190(6)*	*0.205(10)*	0.04(1)
2	0.05(25)	0.01(3)	*0.201(12)*

one can identify the J/ψ state with the lightest in each case, while the ψ' state is the next lightest in two of the cases, but is the third state in the case where the 1^{+-} can contribute. We considered the Z values for the entire set of operators when making the state assignments at finite momentum. This approach becomes increasingly cumbersome as the momentum increases and so we have not considered it any further.

APPENDIX B: IMPROVEMENT OF THE VECTOR CURRENT

In [23] the improvement of the vector current to $\mathcal{O}(ma)$ in a manner compatible with the improvement in the anisotropic clover action was presented. Therein the analysis was for heavy-light currents and the renormalization constants were determined perturbatively. Here we are interested in heavy-heavy currents and we shall determine Z_V nonperturbatively. Nevertheless we can consider modifying our local current to include extra terms suggested by the improvement scheme to investigate any change in the form-factor values. This can be considered to give a crude estimate of how much we might anticipate scaling to the continuum to affect our results.

Our clover action uses $r=1$, and as such our local vector current is not automatically improved—at tree level the improved current is given by $\bar{\Psi}\gamma_\mu\Psi$ where $\Psi(x) \propto (1 + a_s d_1 \gamma_j \vec{D}_j)\psi(x)$ is the "rotated" field used in the construction of the improved action. The improvement parameter $d_1 = \frac{1}{4}(1-\xi r) + \mathcal{O}(m_0 a_t) \approx -0.5$ for renormalized anisotropy $\xi = 3.0$. The quark mass parameter that appears in our clover action, $m_0 a_t$, has the value 0.0401 which is clearly small, while the mass in spatial lattice units is 3 times as large, but still might be argued to be small.

We have attempted to construct the improved current by using the tree-level equation of motion

$$\left(a_t\gamma_4\nabla_4 + a_s\frac{\nu}{\xi_0}\gamma_j\nabla_j + m_0 a_t\right)\psi = 0 \qquad \text{(B1)}$$

to eliminate the derivative in the expansion to $\mathcal{O}(a_s)$ of the improved current $\bar{\Psi}\gamma_\mu\Psi$. This yields the result

$$\bar{\Psi}\gamma_4\Psi \propto \bar{\psi}\gamma_4\psi - d_1 a_s \partial_j(\bar{\psi}\sigma_{j4}\psi), \qquad \text{(B2)}$$

$$\bar{\Psi}\gamma_i\Psi \propto \left(1 - 2m_0 a_t\frac{\xi_0}{\nu}\right)\bar{\psi}\gamma_i\psi - d_1\frac{\xi_0}{\nu}a_t\partial_4(\bar{\psi}\sigma_{i4}\psi), \qquad \text{(B3)}$$

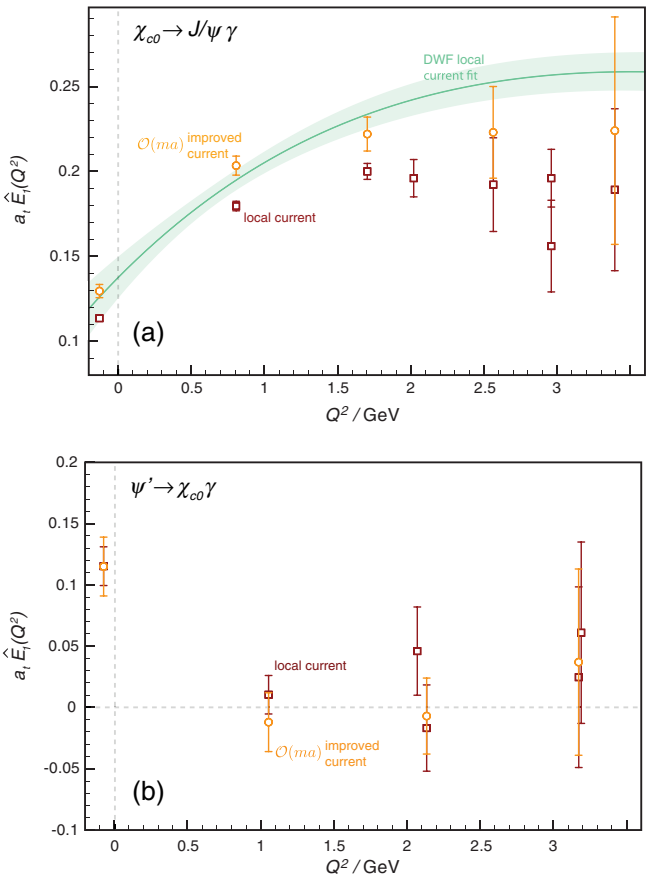

FIG. 16 (color online). Scalar-vector E_1 transition form factors using local and $\mathcal{O}(ma)$ improved current with anisotropic clover quarks and the fit from a study using the local current with domain wall fermions on the same anisotropic lattices. (a) $\chi_{c0} \to J/\psi\gamma$, (b) $\psi' \to \chi_{c0}\gamma$.

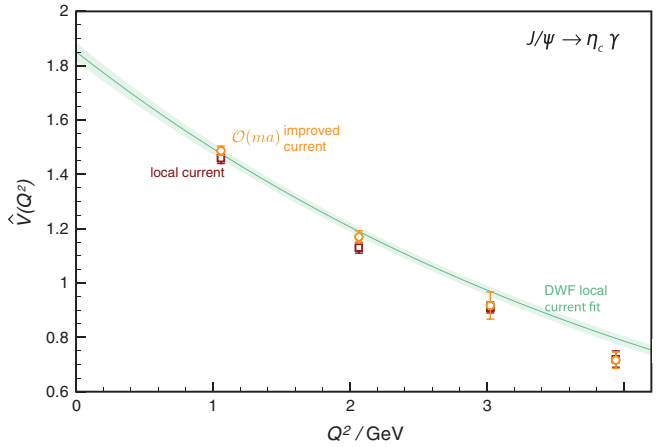

FIG. 17 (color online). $J/\psi \to \eta_c \gamma$ transition form factor using local and $\mathcal{O}(ma)$ improved current with anisotropic clover quarks and the fit from a study using the local current with domain wall fermions on the same anisotropic lattices.

where a common proportionality factor is ignored given that we determine Z_V nonperturbatively using the pseudoscalar form factor at $Q^2 = 0$. At $\vec{q} = (000)$ the second term does not contribute and we would expect $\frac{Z_{V(s)}}{Z_{V(t)}} = 1 - 2m_0 a_t \frac{\xi_0}{\nu} d_1 \approx 1.11$ for the parameters in our action. Note that in Sec. III A we found 1.11(1) for this ratio using a nonperturbative extraction.

We computed form factors using the improved currents for a few of the transitions considered in this paper. The only effect of a considerable size was found in the $\chi_{c0} \to J/\psi\gamma$ transition as shown in Fig. 16(a). Note that the addition of the improvement brings the clover data into better agreement with the domain wall fermion data on the same lattices, as we might expect given the automatic $\mathcal{O}(a)$ improvement one has with domain wall fermion. We note that for the same correlators projected onto the excited state ψ', such a large difference with respect to the local current was not seen; see Fig. 16(b). We were unable to find any other large effects due to improvement; e.g. consider $J/\psi \to \eta_c \gamma$ shown in Fig. 17. These observations may suggest that, except in certain notable cases (the scalar), the discretization errors on our results are relatively small.

[1] J. J. Dudek, R. G. Edwards, N. Mathur, and D. G. Richards, Phys. Rev. D **77**, 034501 (2008).
[2] J. J. Dudek, R. G. Edwards, and D. G. Richards, Phys. Rev. D **73**, 074507 (2006).
[3] J. Gaiser *et al.*, Phys. Rev. D **34**, 711 (1986).
[4] R. E. Mitchell *et al.* (CLEO Collaboration), Phys. Rev. Lett. **102**, 011801 (2009).
[5] T. Barnes and E. S. Swanson, Phys. Rev. C **77**, 055206 (2008).
[6] E. Eichten, K. Gottfried, T. Kinoshita, K. D. Lane, and T.-M. Yan, Phys. Rev. D **17**, 3090 (1978).
[7] E. Eichten, K. Gottfried, T. Kinoshita, K. D. Lane, and T.-M. Yan, Phys. Rev. D **21**, 203 (1980).
[8] G. Li and Q. Zhao, Phys. Lett. B **670**, 55 (2008).
[9] C. A. Meyer, AIP Conf. Proc. **870**, 390 (2006).
[10] F. E. Close and J. J. Dudek, Phys. Rev. Lett. **91**, 142001 (2003).
[11] F. E. Close and J. J. Dudek, Phys. Rev. D **69**, 034010 (2004).
[12] J. J. Dudek and E. Rrapaj, Phys. Rev. D **78**, 094504 (2008).
[13] T. Burch, C. Hagen, C. B. Lang, M. Limmer, and A. Schafer, Phys. Rev. D **79**, 014504 (2009).
[14] B. Blossier, G. von Hippel, T. Mendes, R. Sommer, and M. Della Morte, Proc. Sci., LAT2008 (2008) 135 [arXiv:0808.1017].
[15] C. Amsler *et al.* (Particle Data Group), Phys. Lett. B **667**, 1 (2008).
[16] R. A. Briere *et al.* (CLEO Collaboration), Phys. Rev. D **74**, 031106 (2006).
[17] W. A. Bardeen, A. Duncan, E. Eichten, N. Isgur, and H. Thacker, Phys. Rev. D **65**, 014509 (2001).
[18] T. Barnes, S. Godfrey, and E. S. Swanson, Phys. Rev. D **72**, 054026 (2005).
[19] S. Godfrey and N. Isgur, Phys. Rev. D **32**, 189 (1985).
[20] N. Isgur and J. E. Paton, Phys. Rev. D **31**, 2910 (1985).
[21] P. Guo, A. P. Szczepaniak, G. Galata, A. Vassallo, and E. Santopinto, Phys. Rev. D **78**, 056003 (2008).
[22] P. Chen, Phys. Rev. D **64**, 034509 (2001).
[23] J. Harada, A. S. Kronfeld, H. Matsufuru, N. Nakajima, and T. Onogi, Phys. Rev. D **64**, 074501 (2001).
[24] P. A. Boyle, J. M. Flynn, A. Juttner, C. T. Sachrajda, and J. M. Zanotti, J. High Energy Phys. 05 (2007) 016.
[25] O. Lakhina and E. S. Swanson, Phys. Rev. D **74**, 014012 (2006).
[26] M. G. Olsson, C. J. Suchyta III, A. D. Martin, and W. J. Stirling, Phys. Rev. D **31**, 1759 (1985).
[27] E. J. Eichten, K. Lane, and C. Quigg, Phys. Rev. Lett. **89**, 162002 (2002).
[28] N. Brambilla, Y. Jia, and A. Vairo, Phys. Rev. D **73**, 054005 (2006).
[29] V. A. Beilin and A. V. Radyushkin, Sov. J. Nucl. Phys. **39**, 800 (1984).
[30] F. E. Close and E. S. Swanson, Phys. Rev. D **72**, 094004 (2005).
[31] F. E. Close and C. E. Thomas, Phys. Rev. C **79**, 045201 (2009).
[32] S. Uehara *et al.* (Belle Collaboration), Phys. Rev. Lett. **96**, 082003 (2006).
[33] J. J. Dudek and R. G. Edwards, Phys. Rev. Lett. **97**, 172001 (2006).
[34] E. J. Eichten, K. Lane, and C. Quigg, Phys. Rev. D **69**, 094019 (2004).